

## Article

# Mechanical Characteristics and Acoustic Emission Characteristics of Mortar-Rock Binary Medium

Wenyu Tang <sup>1</sup>, Hang Lin <sup>1,\*</sup>, Yifan Chen <sup>1</sup>, Jingjing Feng <sup>1</sup> and Huihua Hu <sup>2,\*</sup>

<sup>1</sup> School of Resources and Safety Engineering, Central South University, Changsha 410083, China; 165501001@csu.edu.cn (W.T.); 185506005@csu.edu.cn (Y.C.); 195511018@csu.edu.cn (J.F.)

<sup>2</sup> Hunan Provincial Communications Planning, Survey and Design Institute, Changsha 410200, China

\* Correspondence: hanglin@csu.edu.cn (H.L.); huhuihuahnjg@126.com (H.H.)

**Abstract:** The stability of the interface between mortar and rock is very important in engineering construction. In this paper, the all-digital acoustic emission (AE) system is used to detect the direct shear test of the mortar-rock binary medium interface with different sawtooth angles under different normal stress states. The stress-displacement information and AE signal during the whole shearing process are extracted. The coupling relationship between stress and AE characteristic parameters is discussed. The quantitative relationship between sawtooth angle and shear strength of binary medium is established, and three AE characteristic parameters that can be used to predict structural instability are proposed. The research shows that: With the increase of the normal stress and the sawtooth angle, the shear strength of the mortar-rock binary medium increases. The relationship of that is obtained by least squares fitting. The shear stress-displacement curve is divided into five stages according to the change of deformation law. Through the analysis of AE characteristic parameters, it is found that increasing the sawtooth angle makes the AE count and AE cumulative count increase. Based on the analysis of the characteristic parameters of RA-AF, the changes of shear cracks and tensile cracks within the whole shearing process were obtained, respectively. In the process of binary medium shearing, the AE peak frequency is in the range of 120–340 kHz. Three acoustic emission parameters that can predict the macroscopic damage of binary media are obtained: the AE b value, the ratio of shear crack signals, and the number of signals with a peak frequency of 220 Hz to 320 Hz.

**Keywords:** binary medium; sawtooth angle; direct shear test; AE characteristic parameters



**Citation:** Tang, W.; Lin, H.; Chen, Y.; Feng, J.; Hu, H. Mechanical Characteristics and Acoustic Emission Characteristics of Mortar-Rock Binary Medium. *Buildings* **2022**, *12*, 665. <https://doi.org/10.3390/buildings12050665>

Academic Editor: Luca Pelà

Received: 19 April 2022

Accepted: 13 May 2022

Published: 17 May 2022

**Publisher's Note:** MDPI stays neutral with regard to jurisdictional claims in published maps and institutional affiliations.



**Copyright:** © 2022 by the authors. Licensee MDPI, Basel, Switzerland. This article is an open access article distributed under the terms and conditions of the Creative Commons Attribution (CC BY) license (<https://creativecommons.org/licenses/by/4.0/>).

## 1. Introduction

The bond interface between mortar and rock is widely distributed in geotechnical engineering and plays a crucial role in the structure, such as the bond between aggregate and mortar in concrete and the bond between mortar and surrounding rock in the anchoring system are the key factors to system carrying capacity [1–3]. Once the bonding of the interface is destroyed, it will lead to concrete cracking, instability, and failure of the bolt support. Therefore, it is of great importance to study the action mechanism of the mortar-rock interface. In recent years, the research on the rock-mortar interface has mainly focused on the crack propagation and mechanical properties of the interface between concrete aggregate and mortar [4–6]. LYBIMOVE and Pinns [7] proposed the concept of interfacial transition zone (ITZ), and the structural properties of ITZ are the main factors determining the mechanical properties of concrete. Qiu [8] proposed a rock-mortar dual-material Brazilian disk configuration and simulated the ITZ failure process of the dual-material specimen. Dynamic direct tensile properties of concrete are related to mortar strength and ITZ strength, and an empirical formula denotes the dynamic increase factor of tensile fracture energy of concrete [9]. The effect of aggregates on the fracture parameters of high-performance concrete was studied through experiments and acoustic emission techniques by Chen and Liu [10]. The dynamic fracture characteristics of the mortar-rock

specimens were studied, and the crack propagation time and velocity were measured by Qiu [11]. A crack propagation criterion for layered mortar-rock beams is presented, and a numerical method for predicting the crack propagation process is presented by Wang [12]. Based on the bending strength and fracture energy, the relationship between the fracture parameters and the mechanical properties of the mortar-rock interface is revealed by Satoh [13]. In addition, most of the studies on the bonding effect of the anchoring interface are based on static or dynamic mortar push-out tests [14,15]. The operation of the mortar push-out test is simple and convenient, but sometimes the matrix cracks, which affects the test results. In contrast, the direct shear test under constant normal stress can effectively avoid the occurrence of matrix cracking [16–19]. Although the above study deepens the understanding of interface fracture and failure of binary media to a certain extent, they have not paid much attention to the roughness of the mortar-rock interface. In fact, the roughness of the interface also has a great influence on the bonding effect of the two-material interface and the shear characteristics of the structure [20–23]. Therefore, it is necessary to explore the effect of the roughness of the binary medium interface. In addition, the acoustic emission monitoring technology can analyze the changes of the acoustic emission characteristic parameters when the internal cracks develop in the specimen, judge the nature of the cracks, and give an early warning of the macroscopic damage which is a powerful tool to conduct failure characteristic [24,25]. A more comprehensive analysis of the shear behavior of rock-mortar binary medium using the acoustic emission monitoring technology and considering the roughness of the interface will be carried out in this paper.

In this paper, the direct shear test of the mortar-rock binary medium is carried out. The interface of specimens is serrated with four different sawtooth angles, and the tests are carried out under the constant normal stress of five levels. The shear process is monitored by a fully digital acoustic emission system, and the characteristic parameters and shear stress of shear acoustic emission are coupling analyzed. The influence of normal stress and interface roughness on the interface shear characteristics is revealed, and the interface instability failure is reasonably predicted, which provides a basis for various geotechnical engineering construction and design.

## 2. Materials and Methods

In order to study the effect of roughness on the shear characteristics of the binary medium of mortar and rock, the engraving machine was used to engrave 10 sawtooths on the rock surface. As shown in Figure 1, the sawtooth angle is set to 8°, 30°, 45°, and 55°, and the size of the rock is 70 mm, 70 mm, and 35 mm in length, width, and height, respectively. After the rock is processed, it is poured on the serrated surface of the rock with the prepared cement mortar, the cement (Hunan Ningxiang Nanfang Cement Co., LTD, Hunan Ningxiang, China) grade is 42.5, and the particle size of the river sand is less than 0.5 mm. The ratio of cement, sand, and water by weight are 2:1:0.6, and the size of the specimen after pouring is 70 mm × 70 mm × 70 mm (as shown in Figure 2). The rock selected for this test is greywacke from Hunan, China, which is a relatively uniform sedimentary rock with relatively stable mechanical properties. The uniaxial compressive strength of the rock is 72 MPa, the bond force is 9 MPa, and the internal friction Angle is 61.8°. The uniaxial compressive strength of mortar is 15.6 MPa, the bond force is 3.12 MPa, and the internal friction Angle is 60.4°.

As shown in Figure 3, the direct shear test under constant normal stress was carried out by the YZW100 multifunctional rock direct shear instrument developed by Jinan Mining and Rock (Jinan, Shandong, China). According to the rock physical property test procedures [26], the normal stress should not be lower than the design stress, the normal stress in this test is set to 1 MPa, 2 MPa, 3 MPa, 4 MPa, and 5 MPa respectively. In order to make the shear loading element contact the specimen quickly, the shear loading adopts the combined loading mode of pre-control and displacement control, that is, when the pre-control shear force reaches 1 KN, it is switched to the displacement control loading mode, and the loading speed is 0.01 mm/s.

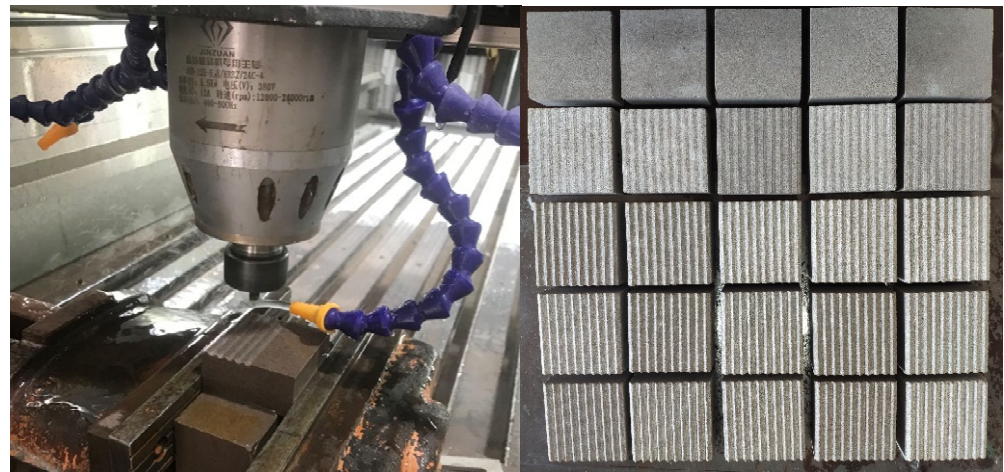


Figure 1. Processing of rock surface.

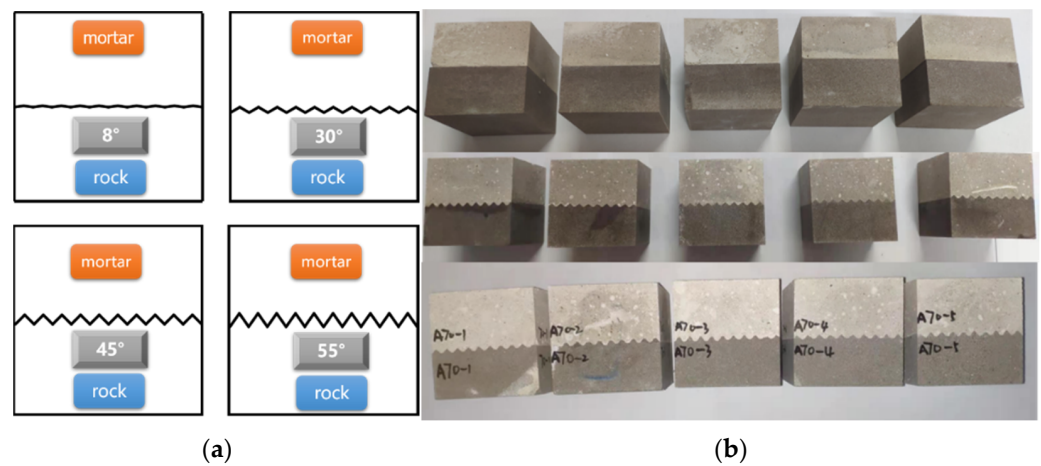


Figure 2. Specimen preparation before direct shear test. (a) Schematic diagram of specimens with different sawtooth angles. (b) Specimens after pouring.

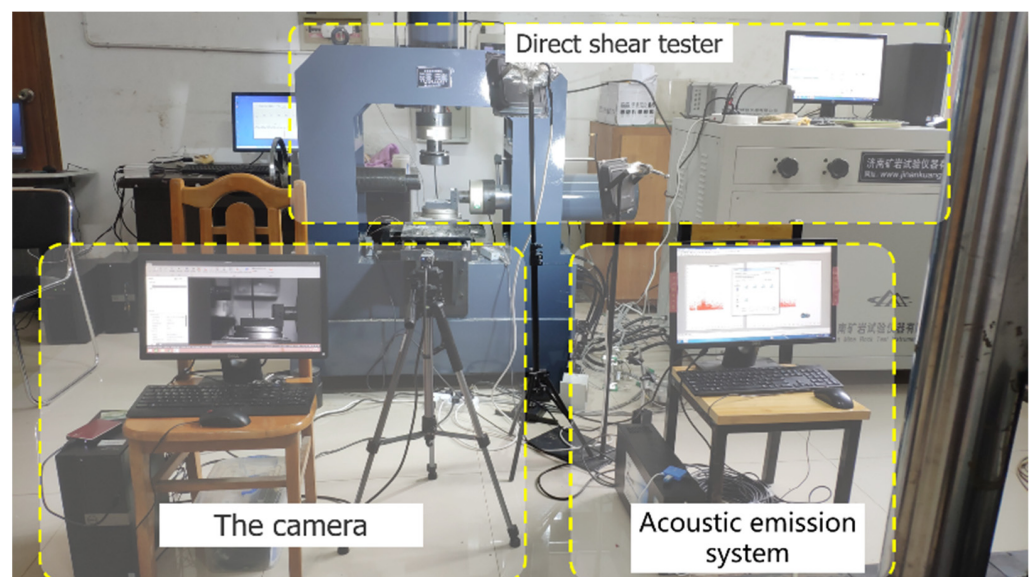
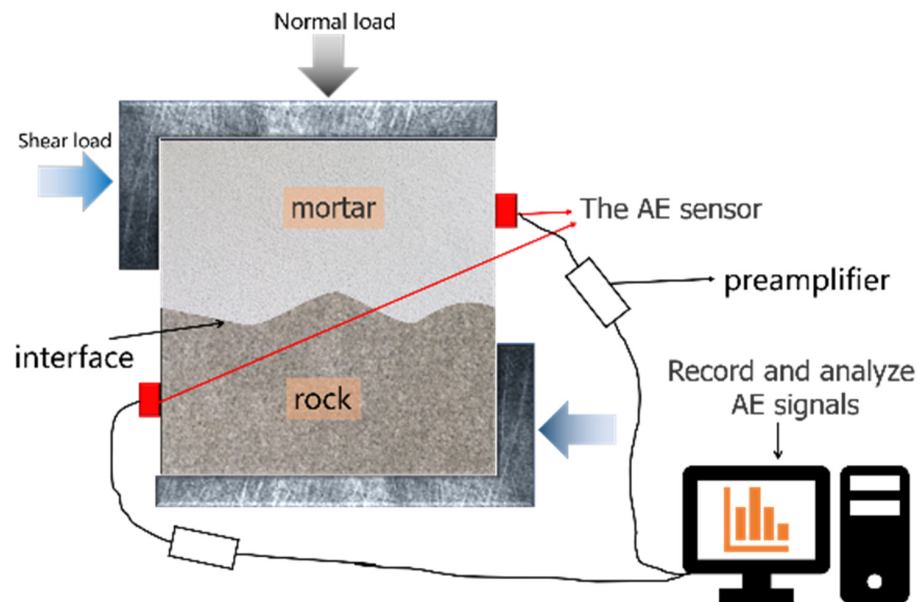


Figure 3. Shearing instrument, acoustic emission system.

AE monitoring is carried out during the shearing process. The position of the AE sensors and the signal acquisition process is shown in Figure 4. The AE monitoring system used in this paper is a 16-channel fully digital acoustic emission system. AE signals were detected by two AE sensors and the sampling frequency for recording wave-forms was 10 MHz. AE waves were amplified with 40 dB gain by a pre-amplifier. AE sensors were attached to the surface of the specimen with vaseline, so that the sensor face and the specimen surface have a good contact for the signal detection. The thresh-old level is 45 dB.



**Figure 4.** Schematic diagram of acoustic emission signal acquisition system.

### 3. Test Results and Analysis

#### 3.1. Shear Mechanics Characteristics of Mortar-Rock Binary Medium

In order to compare the difference in shear mechanical properties of rock and mortar rock binary media, direct shear tests were carried out on intact rock and binary media samples, respectively. The intact rock sample size, normal stress, and shear rate are all the same as those of the binary medium sample. The shear stress-displacement relationship of rock and binary medium is shown in Figures 5 and 6.

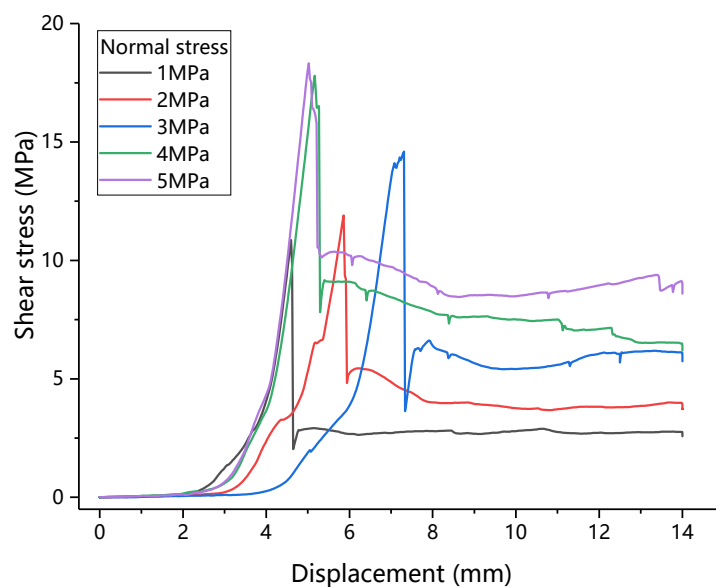
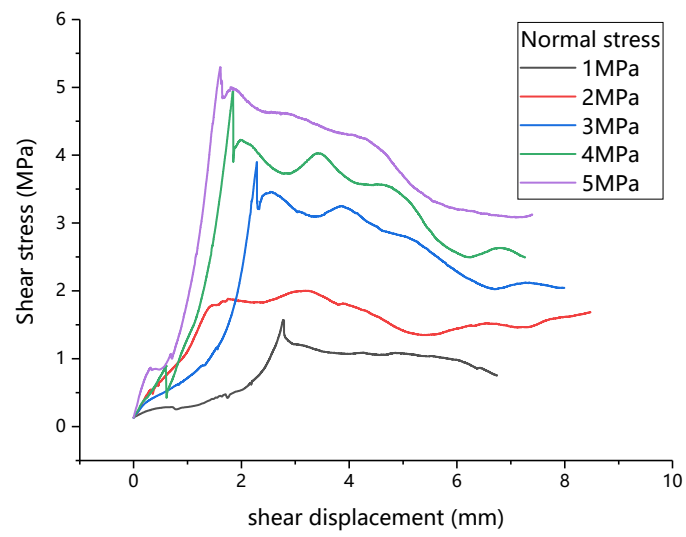
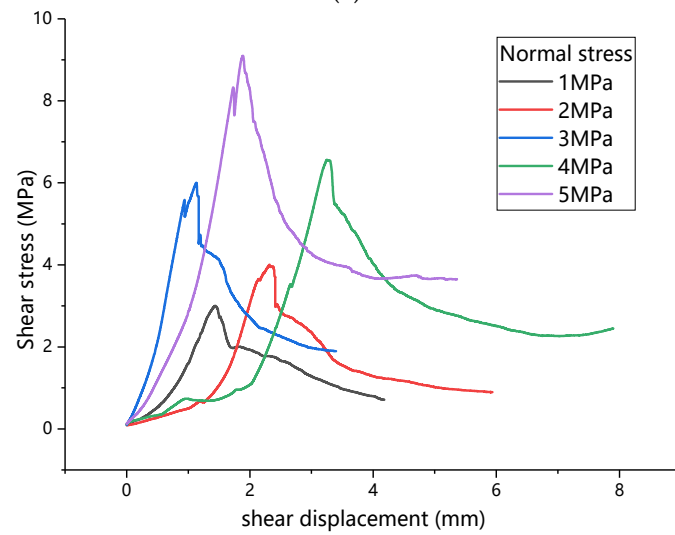


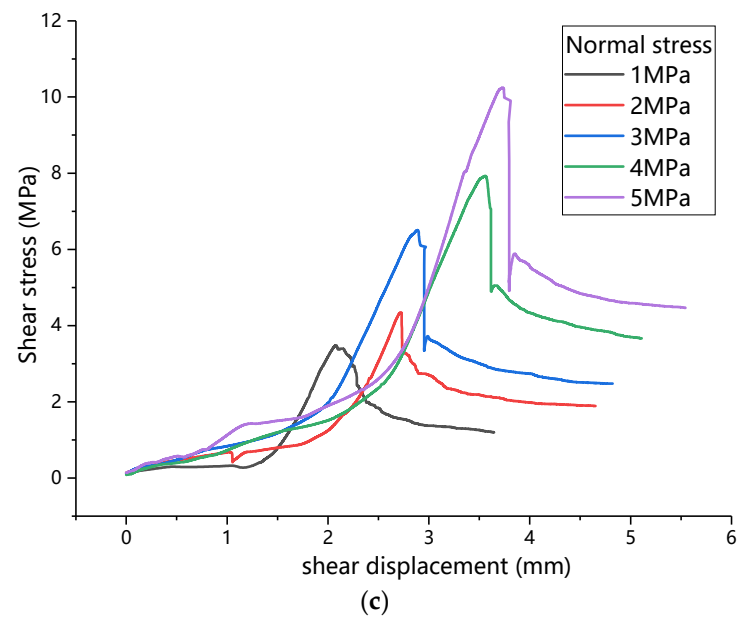
**Figure 5.** Relationship between shear stress and shear displacement of rock.



(a)

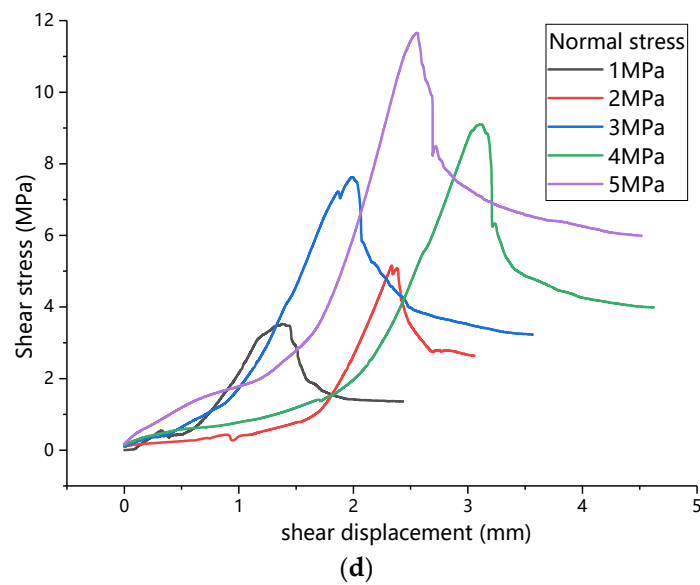


(b)



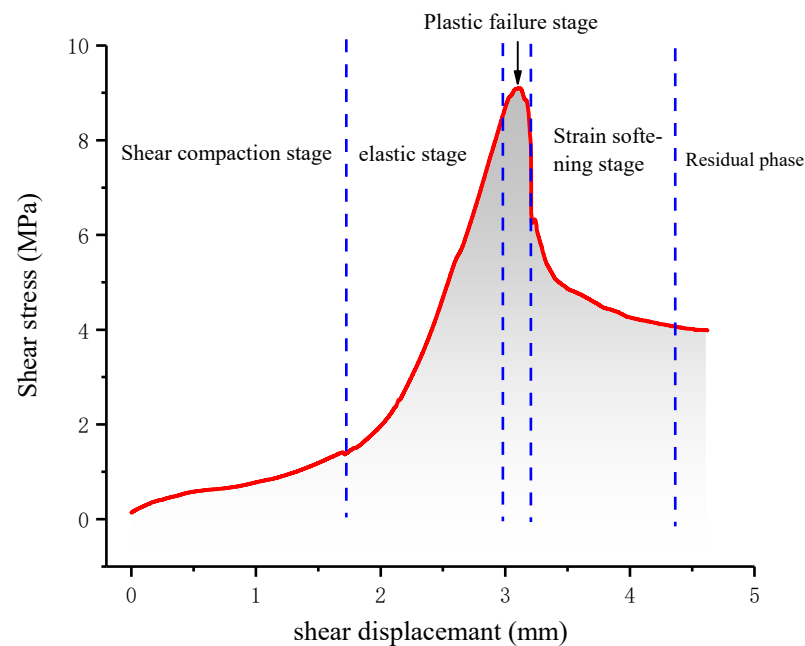
(c)

Figure 6. Cont.



**Figure 6.** Relationship between shear stress and shear displacement of mortar-rock binary medium. (a) 8° (b) 30° (c) 45° (d) 55°.

Figure 5 shows that the intact rock exhibits elastic-brittle failure in shear, and the shear stress before failure is linearly related to the shear displacement. In order to easily reflect the shear stiffness of rocks and binary media, the value of  $k$  is defined as the ratio of the change of shear stress to the change of shear displacement in the elastic section, that is,  $k = \Delta\tau/\Delta\delta$ , in MPa/mm, and  $k'$  is the ratio of shear stress change to shear displacement change before the elastic stage. According to the change in shear stiffness, the shear curve can be divided into five stages: the shear compaction stage, the elastic stage, the plastic failure stage, the strain softening stage, and the residual stress stage, as shown in Figure 7.



**Figure 7.** Stages of the shearing process.

In order to study the effect of roughness on the shear characteristics of the binary medium under different normal stress, direct shear tests were carried out on the mortar-rock binary medium with sawtooth angles of 8°, 30°, 45°, and 55°, the relationship between shear displacement and shear stress is obtained, as shown in Figure 6. It can be seen from

Figure 6 that with the increase of shear displacement, the shear stress first increases, then decreases, and finally tends to remain unchanged.

During the shear compression stage, the slope of the curve increases gradually and does not change after entering the elastic phase. Due to the different shear stiffness of mortar and rock, the deformation of the two materials is inconsistent when the binary medium is under the same external force. As the shear displacement increases, the deformation of the two materials is coordinated, and then the specimen enters the elastic stage, and the two materials jointly provide shear resistance, so the slope of the curve does not change.

In the plastic failure stage, both the sawtooth angle and the normal stress affect the failure mode of the binary medium. In the case of a small sawtooth angle, as shown in Figure 6a, two stress peaks appear in the curve, the stress drops rapidly after the first peak and decreases gently at the second peak. The failure mode of the specimen is brittle failure followed by plastic failure. Brittle failure occurs when the mortar and rock cementation surface are separated, and the subsequent ductility fluctuation is the plastic failure caused by slip friction. In the case of a large sawtooth angle, as shown in Figure 6c,d, the curve quickly drops after reaching the peak value and enters the residual stress stage. The specimen showed brittle failure, and the greater the normal stress, the more obvious the brittle failure phenomenon. When the sawtooth angle and normal stress are large, the sawtooth on the mortar side is prone to shearing damage.

Table 1 summarizes the  $k$  values of the binary medium samples and intact rocks. The relationship between the  $k$  value and normal stress is plotted in Figure 8. It can be seen from Figure 8. that with the increase of normal stress, the  $k$  values of rock and binary medium show an upward trend, and the  $k$  value of rock is greater than that of the binary medium. The sawtooth angle has little effect on the  $k$  value of the binary medium, but the increase of the normal stress has a stronger compacting effect on the micro-cracks in the specimen, so it has an increasing effect on the shear stiffness of the specimen. The mortar-rock binary medium is worse than the intact rock in terms of density and integrity, so its shear stiffness is much smaller than that of the intact rock.

**Table 1.**  $k$  value under different normal stress.

Normal Stress	The Value of $k$				
	Sawtooth Angle of 8°	Sawtooth Angle of 30°	Sawtooth Angle of 45°	Sawtooth Angle of 55°	Intact Rock
1 MPa	1.74	3.46	5.72	5.61	12.01
2 MPa	1.75	4.83	6.07	7.21	13.23
3 MPa	5.85	8.06	5.79	8.03	15.58
4 MPa	6.45	5.67	6.26	8.82	16.21
5 MPa	6.92	9.29	8.02	11.59	18.56

In order to analyze the influence of the serration angle before the elastic stage on the shear stiffness, the  $k'$  value was calculated for the shear results of the binary medium with different serration angles under the normal stress of 2 MPa. The ratio of  $k'$  to  $k$  reflects the shear stiffness before the elastic stage. Figure 9 shows the relationship between shear displacement and the ratio. It can be seen from Figure 9. that with the increase of shear displacement, the ratio first increases slowly, then suddenly rise, and lastly remains the same. The change in the ratio indicates that the shear stiffness has changed, and the shear transitions from the shear compression stage to the elastic stage. We use this as the basis for dividing the shear compression stage and the elastic stage in the shear process. With the increase of the sawtooth angle of the binary medium, the displacement corresponding to the sudden change of the ratio is larger, which indicates that the greater the roughness of the interface of the binary medium, the later the specimen transitions to the elastic stage.

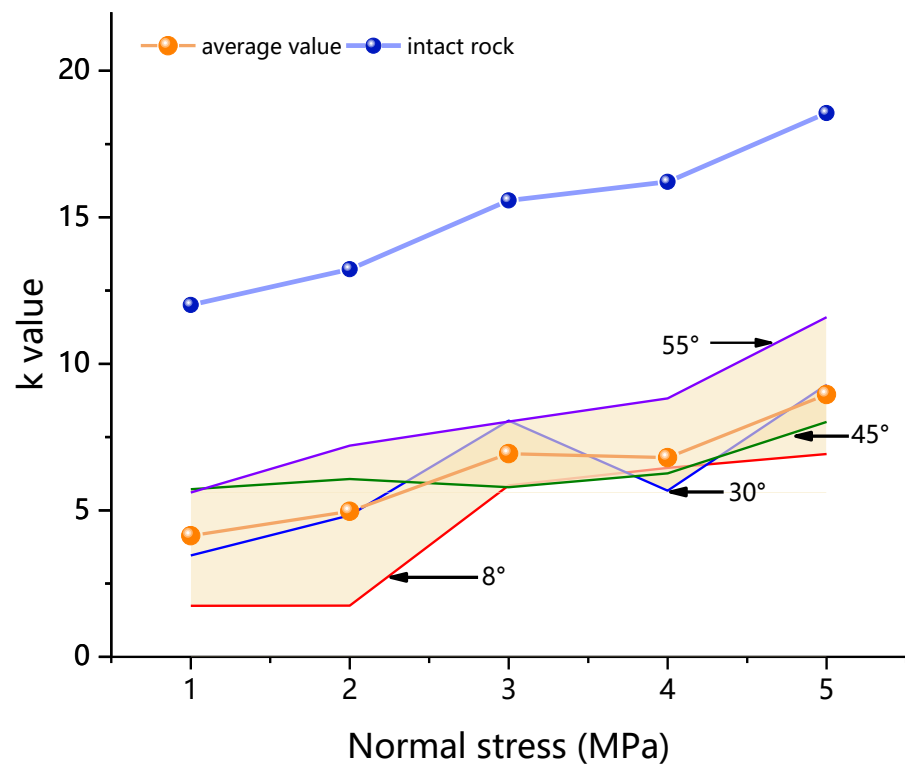


Figure 8. Relationship between normal stress and k value.

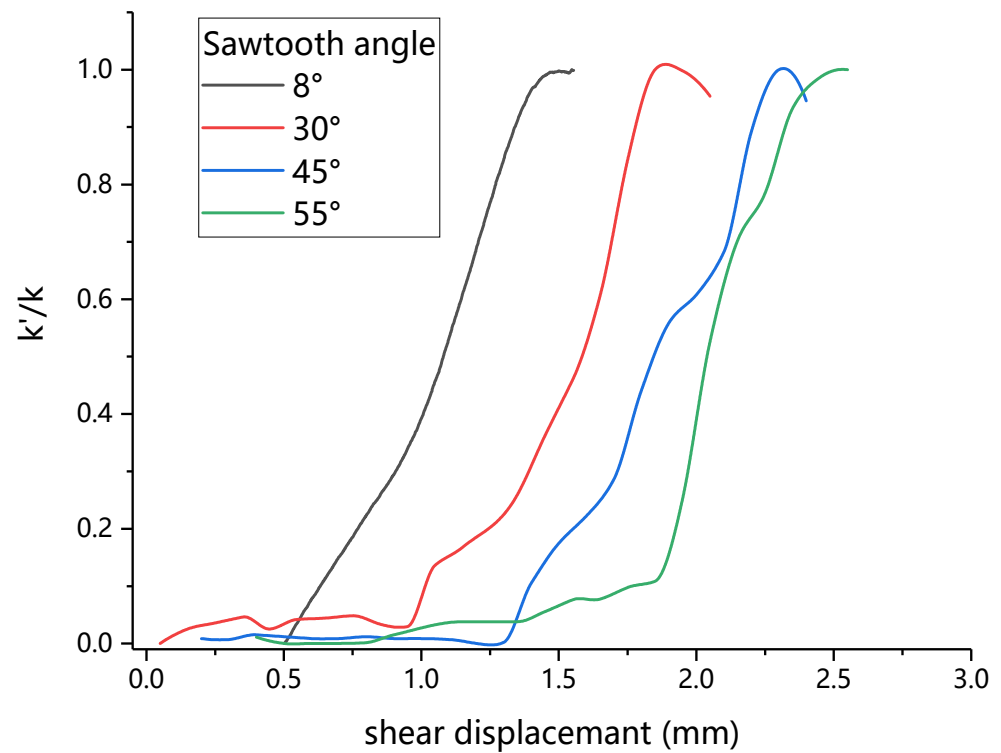


Figure 9. The relationship between shear displacement and  $k/k'$ .

In order to study the effect of sawtooth angle and normal stress on the shear strength of binary media, the shear strength of specimens with different sawtooth angles under different normal stresses is shown in Figure 10. It can be seen from the Figure that with the increase of normal stress and sawtooth angle, the shear strength increases. According

to the Mohr-Coulomb criterion, the relationship between the normal stress and the shear stress at each sawtooth angle in Figure 10 can be linearly fitted to obtain the cohesive force and internal friction angle of the rock and mortar-rock binary medium. The cohesive force of the rock is 9 MPa, and the internal friction angle is  $61.8^\circ$ , as shown in Figure 11.

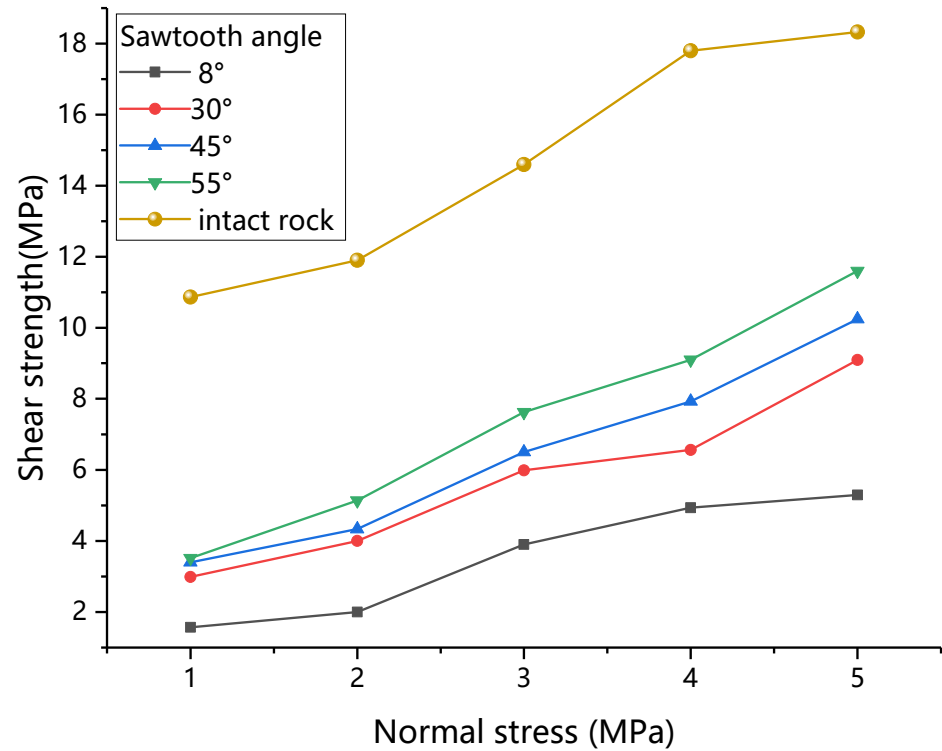


Figure 10. Relationship between normal stress and shear strength of rock and binary medium.

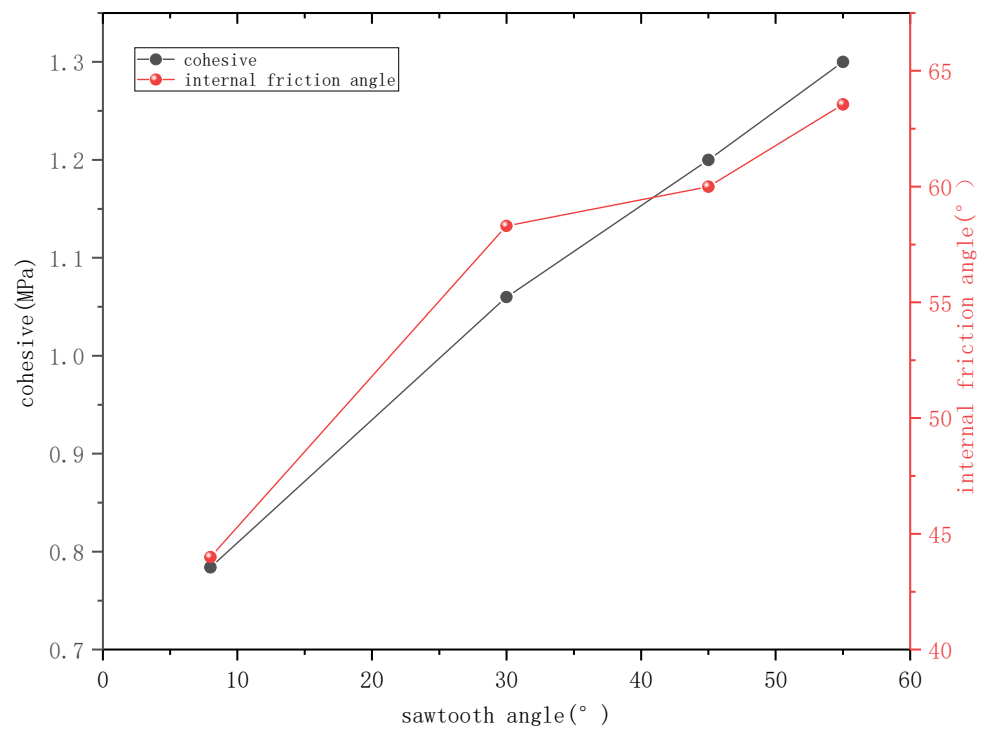


Figure 11. Relationship between cohesive force, internal friction angle and sawtooth angle.

With the increase of the sawtooth angle, the cohesive force, and the internal friction angle of the binary medium both increase. The cohesive force of the binary medium is much lower than that of the complete rock, which is caused by the weakness of the cemented surface of the binary medium, and the cemented interface is easily damaged such as dislocation and separation. This is also the reason why the binary medium is very important for structural stability in rock mass engineering. It can be seen from Figure that the internal friction angle of the sample with the sawtooth angle of 30–55° is close to that of the rock, but the internal friction angle is very small at 8°. This is because the sawtooth angle is very small, the binary medium is mainly in the interface separation and slip failure mode, and the friction between the mortar and the rock provides the main shearing effect. With the increase of the sawtooth angle, the structural surface is mostly damaged by partial or complete shearing of the sawtooth, and the mortar and rock bear more shear resistance. Therefore, a piecewise function is used to fit the relationship between the sawtooth angle and the internal friction angle of the binary medium, and the relationship between the internal friction angle and the sawtooth angle is obtained, as shown in formula (1). Equation (2) is obtained by linear fitting between the cohesive force of the binary medium and the tangent of the sawtooth angle. According to the Mohr-Coulomb criterion, the relationship between the shear strength of the mortar-rock binary medium, the normal stress, and the sawtooth angle of the structural plane can be obtained, as shown in Equation (3).

$$\theta(\alpha) = \begin{cases} a_1 + k_1\alpha, & \alpha < \alpha_i \\ \theta_i + k_2(\alpha - \alpha_i), & \alpha \geq \alpha_i \end{cases} \quad (1)$$

where  $\theta$  is the internal friction angle of the binary medium,  $\theta_i = a_1 + k_1\alpha_i$ ,  $\alpha_i = 31.5$ ,  $a_1 = 39.1$ ,  $k_1 = 0.609$ ,  $k_2 = 0.2234$

$$C(\alpha) = a + b \tan(\alpha) \quad (2)$$

where  $C$  is the cohesive force of the binary medium.  $a = 0.78$ ,  $b = 0.4$ .

$$\tau = C(\alpha) + \sigma_n \tan(\theta(\alpha)) \quad (3)$$

In the residual stage, the shear stress-displacement curve of the binary medium basically remains unchanged at the residual stress. Figure 12 shows the relationship between the residual strength of the specimens and the normal stress. It can be seen from the Figure that with the increase of the normal stress, the residual strength of the binary medium tends to increase. According to the Mohr-Coulomb criterion, the residual internal friction angle of binary media with different roughness is obtained. Figure 13 shows the relationship between the sawtooth angle and the residual internal friction angle. It can be seen from the Figure that the residual internal friction angle of the binary medium is in the range of 30–48°, and increases with the increase of the sawtooth angle. The larger the sawtooth angle, the greater the roughness of the contact interface after shearing is, which provides a greater bearing capacity in the residual stage. Interestingly, the residual internal friction angle of the specimen with the sawtooth angle of 55° is larger than the internal friction angle of the specimen with the sawtooth angle of 8°. It shows that when the sawtooth angle is large, even if the structure is damaged, the residual bearing capacity of the binary medium is larger than that of the small sawtooth angle binary medium without damage.

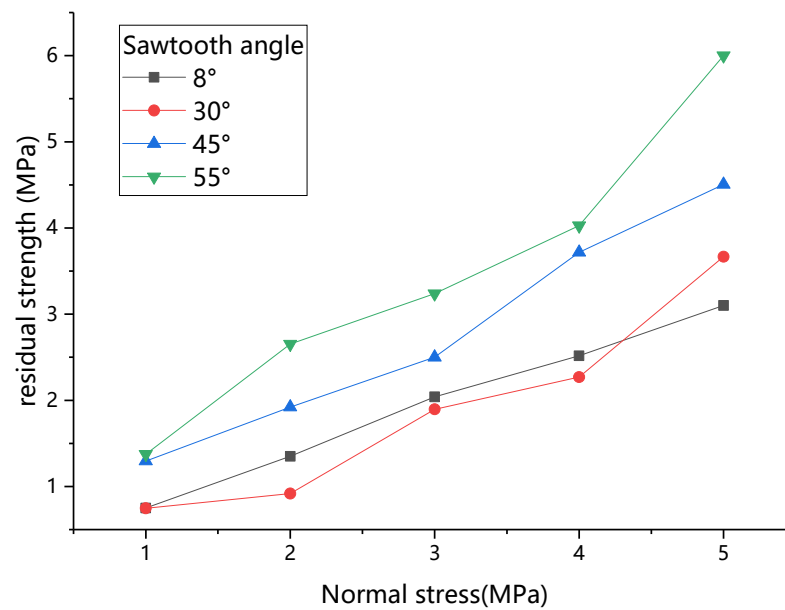


Figure 12. Relationship between normal stress and residual strength.

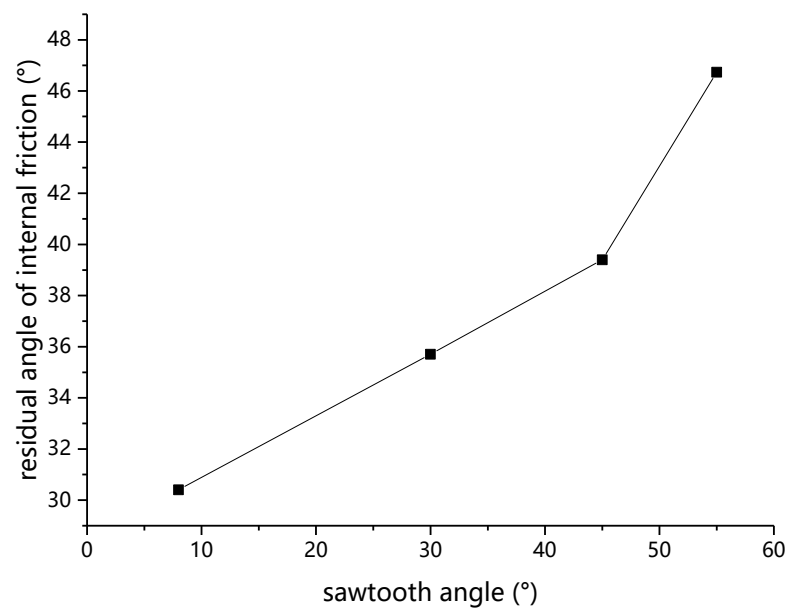


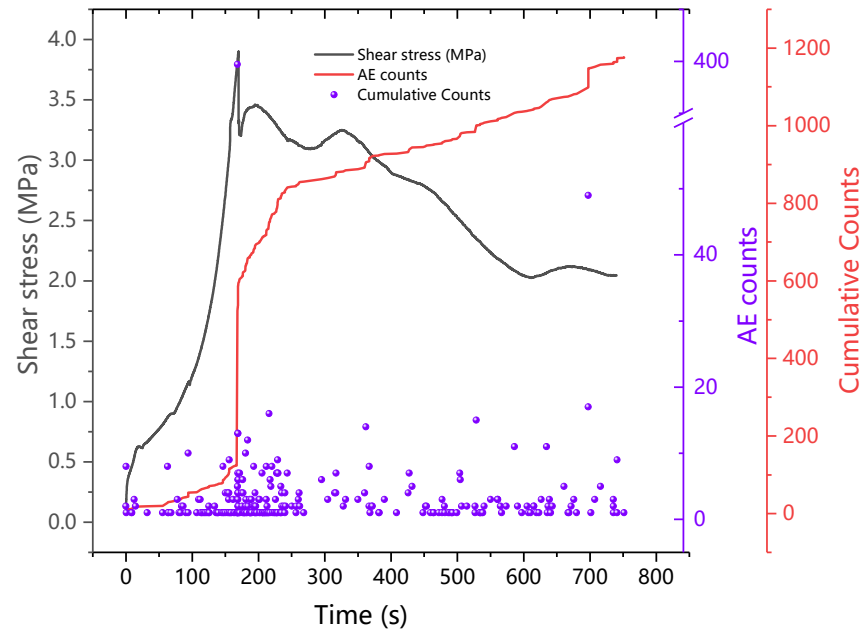
Figure 13. Relationship between sawtooth angle and residual internal friction angle.

### 3.2. Analysis of Acoustic Emission Characteristic Parameters

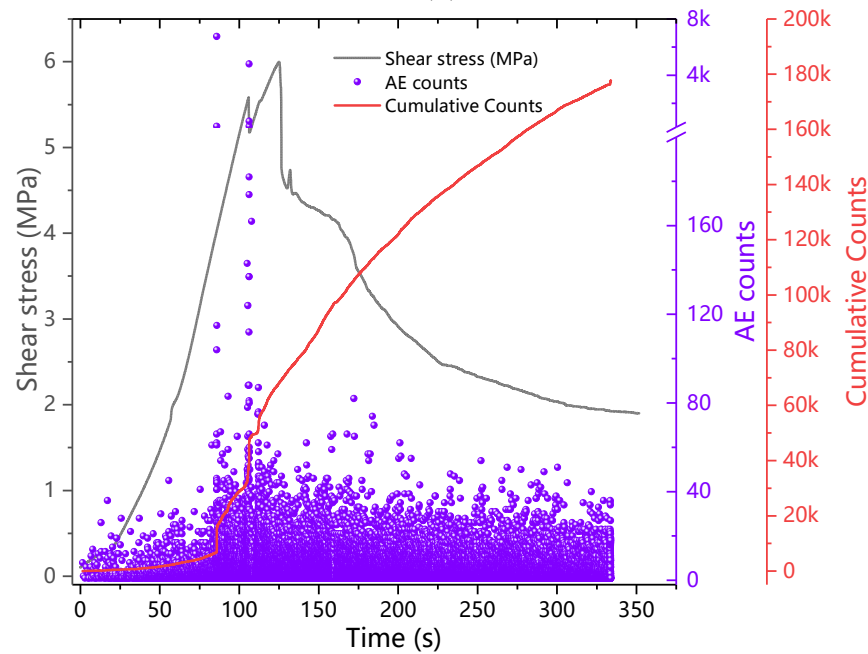
#### 3.2.1. AE Counts

AE counts is the number of times the AE signal excursions over the AE threshold. Figure 14 shows the relationship between AE counts, AE cumulative counts, and time during the shearing process of the binary medium with different sawtooth angles under the normal stress of 3 MPa. It can be seen from the Figure that in the shear compaction stage and the elastic stage, the AE count is low, and the AE cumulative counts increase slowly, which indicates that the internal cracks of the specimen develop slowly before failure. In the failure stage, super large AE counts appeared, and the AE cumulative counts increased suddenly, which indicated that the micro-cracks in the specimen rapidly expanded and penetrated each other during the failure stage, forming macroscopic failure. In the residual stage, the AE counts dropped, but were generally higher than those before shear failure, and the cumulative AE counts showed a rapid growth pattern. The main failure mode of

the specimen in the residual stage is sliding friction failure, which is more severe than the acoustic emission in the elastic stage and the shear compaction stage, but there is almost no development and penetration of micro-cracks. Comparing Figure 14a–d, it can be found that the greater the interface roughness of the binary medium, the greater value of the AE counts and the AE cumulative counts. The increase of the sawtooth angle makes the shear damage more severe, and the AE signal is easier to monitor.



(a)



(b)

Figure 14. Cont.

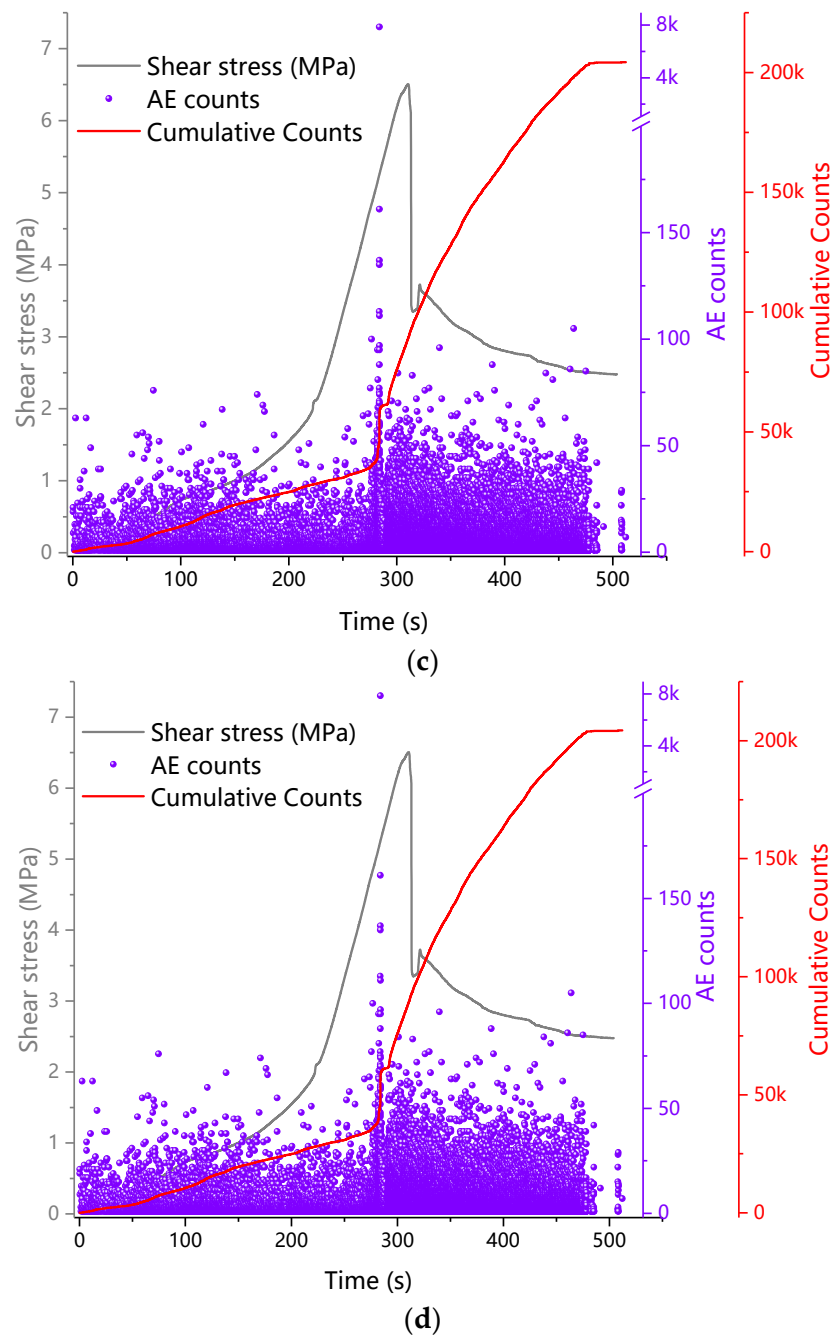


**Figure 14.** Relationship between AE counts, AE cumulative counts and time. (a) 8° (b) 30° (c) 45° (d) 55°.

### 3.2.2. b Value

The b value is an important parameter derived from seismology, and its application in the AE technology of geotechnical mechanics can reflect the degree of crack propagation inside the material. When the crack propagation scale is large, the acoustic emission b value is small, and when the crack propagation scale is small, the acoustic emission b value is large. The b value is calculated by Equation (4) [27].

$$\log N = a - bM \quad (4)$$

In which,  $M$  is the AE amplitude, in dB;  $N$  is the number of amplitudes within the range of the amplitude  $M$  and  $M + dM$ ;  $a$ ,  $b$  are constants.

In this paper, the self-compiled MATLAB program is used to calculate the  $b$  value in the shearing process of binary media with different sawtooth angles, and the relationship between time and  $b$  value is plotted in Figure 15. It can be seen from the Figure that in the shear compaction stage and the elastic stage, the  $b$  value increases slowly or does not change, indicating that in these two stages, the formation and expansion of tiny cracks mainly occur inside the specimen but have not yet penetrated. In the failure stage, the  $b$  value dropped suddenly, indicating that a large number of micro-cracks penetrated through the specimen to form macro-cracks, and caused the instability of the structure. In the residual stage, the  $b$  value of acoustic emission varies greatly, but the overall trend is gradually increasing, indicating that the proportion of large-scale cracks in the specimen decreases. Observing the relationship between the change of the  $b$  value and the shear stress in the figure, before the shear stress reaches the peak value, the AE  $b$  value will drop suddenly, indicating that the sudden drop of the  $b$  value can provide an early warning for the macroscopic damage of the structure.

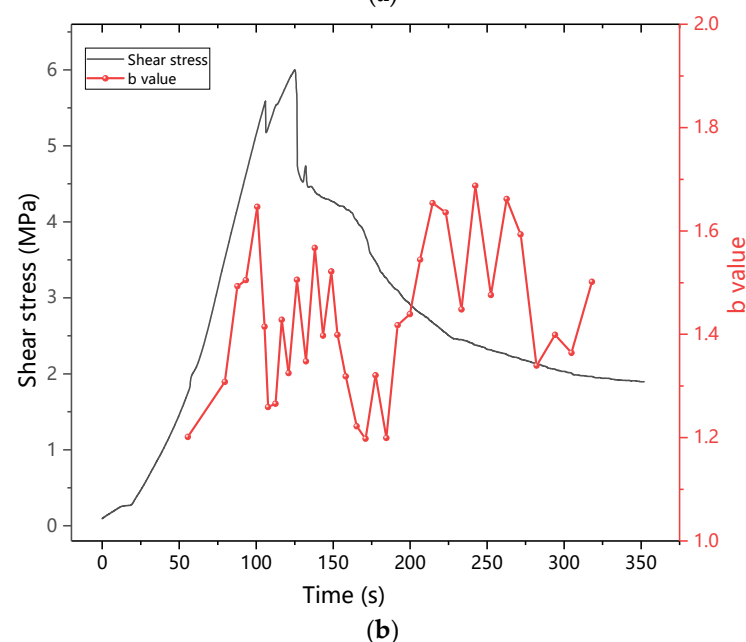
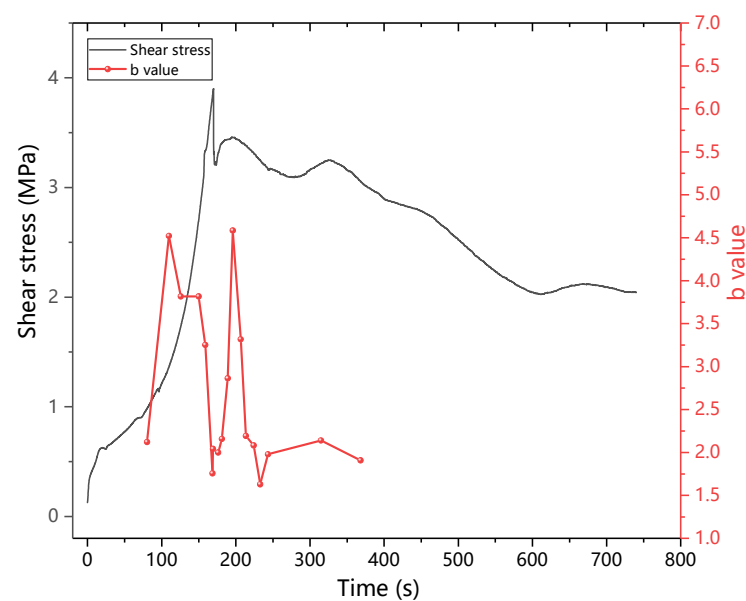
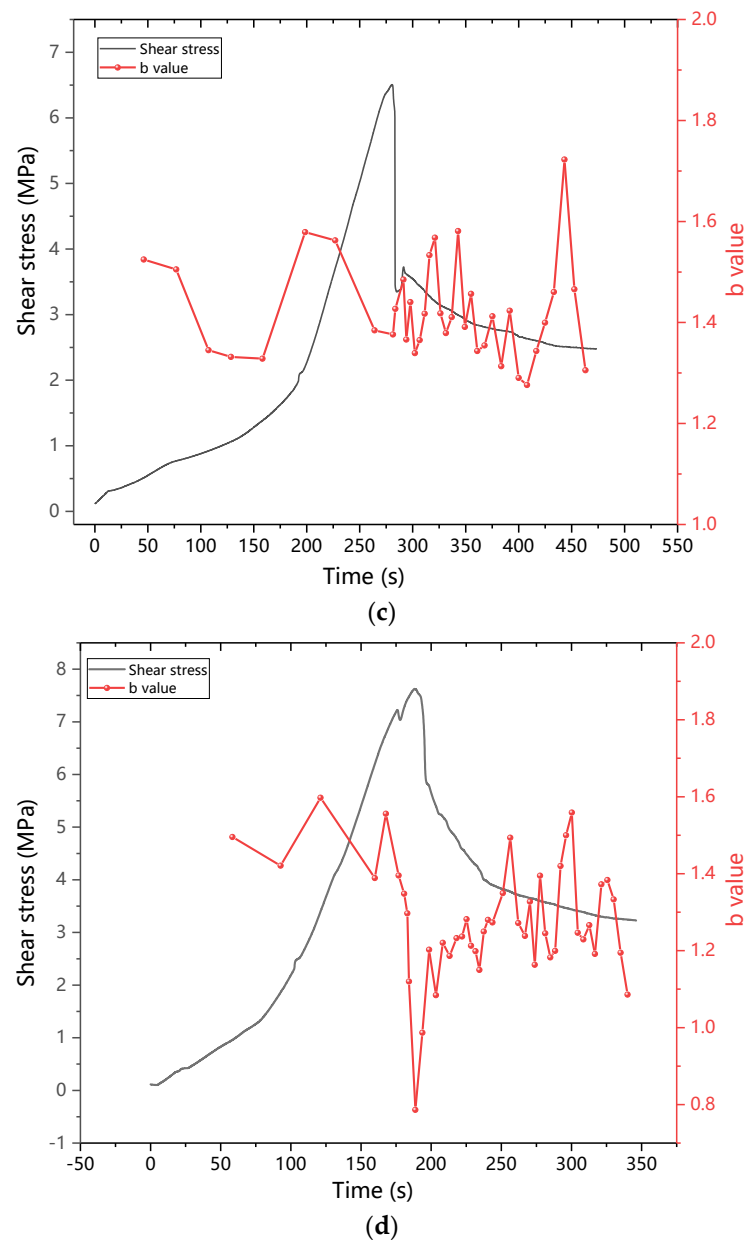


Figure 15. Cont.



**Figure 15.** Relationship between AE b value and time in the whole shearing process. (a) 8° (b) 30° (c) 45° (d) 55°.

### 3.2.3. Crack Identification Analysis

According to the Japanese standard JCMS-III B5706 [28], as shown in Figure 16, tensile cracks and shear cracks can be distinguished by two parameters, AF and RA. The slope of the dividing line is defined as  $r$ , and the signal is defined as shear failure signal, the signal with  $AF/RA > r$  is defined as tension failure signal, and the  $r$  value is between 0–200. AF is the average frequency, which is the ratio of ring count to duration in kHz. RA is the ratio of AE rise time to AE amplitude, Equation (5) [29], in ms/V. The maximum voltage value of the AE signal can be converted from the AE amplitude, as shown in Equation (5).

$$RA = \frac{T}{V_{max}} = \frac{T}{10^{A/20}} \quad (5)$$

The  $T$  is the rise time,  $V_{max}$  is the maximum voltage value in  $\mu V$ , and  $A$  is the amplitude in dB.

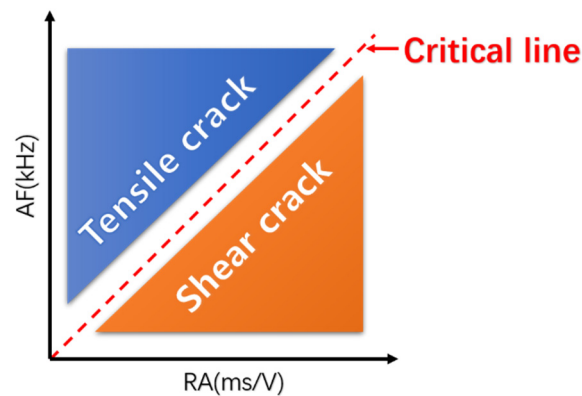


**Figure 16.** Schematic diagram of crack distinction.

In order to analyze the development of tensile and shear cracks in the shearing process of the mortar-rock binary medium with different sawtooth angles, the relationship between RA and AF in the shearing process of four kinds of roughness binary mediums is shown in Figure 17, respectively. In this paper, based on previous experience [30–32], the value of  $r$  is set to 50, it can be seen from the Figure that most of the signals are distributed below the critical line, that is, the shear crack acoustic emission signal is dominant in the entire shearing process. As the sawtooth angle increases, more signal points of obvious shear cracks are shown in the figure. (High RA value, low AF value). Figure 18 shows the change in the RA value during the shearing process. It can be seen from the Figure that the RA value is evenly distributed in the low area during the shear compaction and elastic stages. In the plastic failure stage, the RA value suddenly increased to a peak value, and the signal was denser, indicating that the shear cracks in the specimen developed and penetrated rapidly during this stage. In the residual stage, the RA value of acoustic emission is mostly reduced, and the distribution range is larger than the RA value of the shear stage and the elastic stage. This indicates that in the residual stage, frictional slip between the two mediums occupies the dominant failure mode.

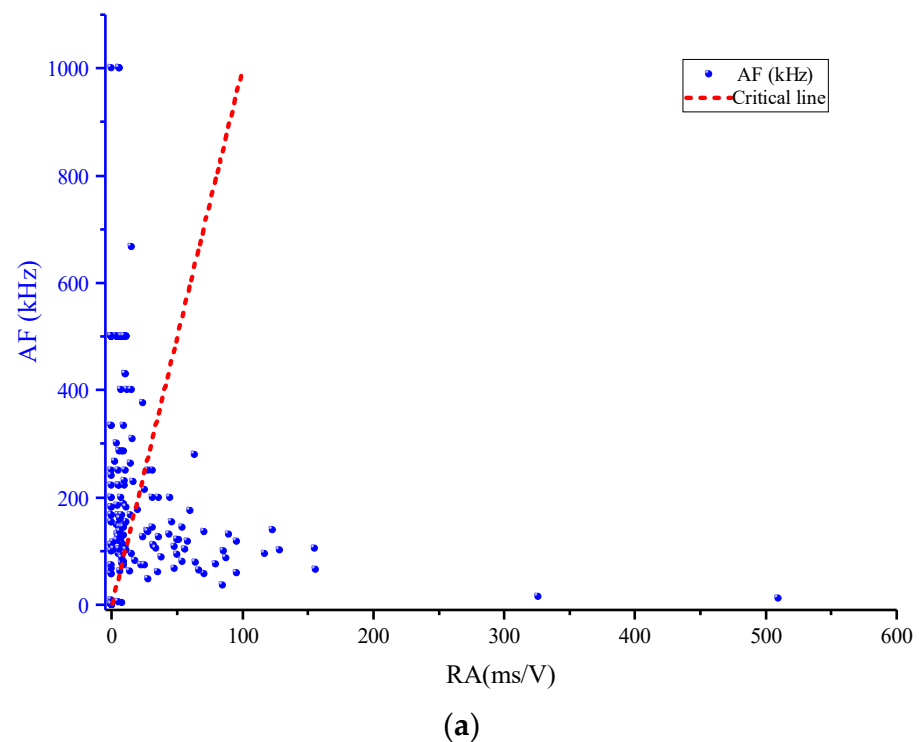
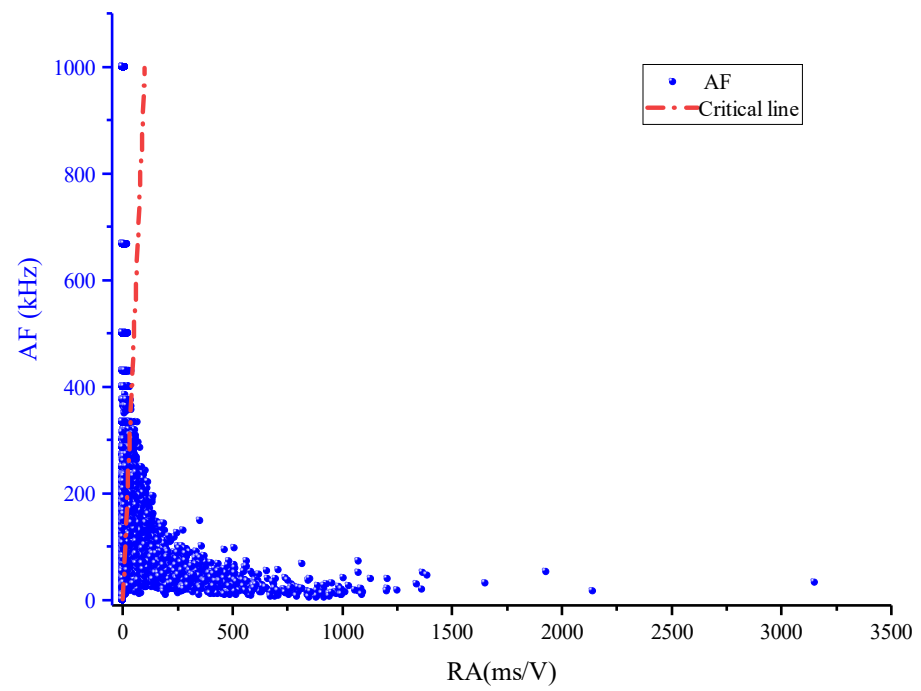
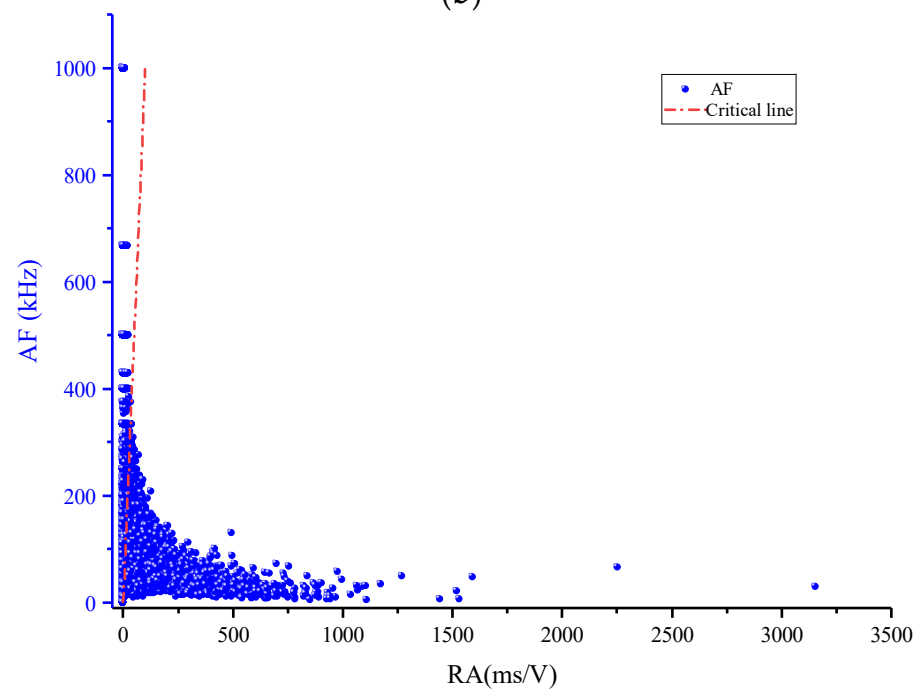


**Figure 17.** Cont.



(b)



(c)

Figure 17. Cont.

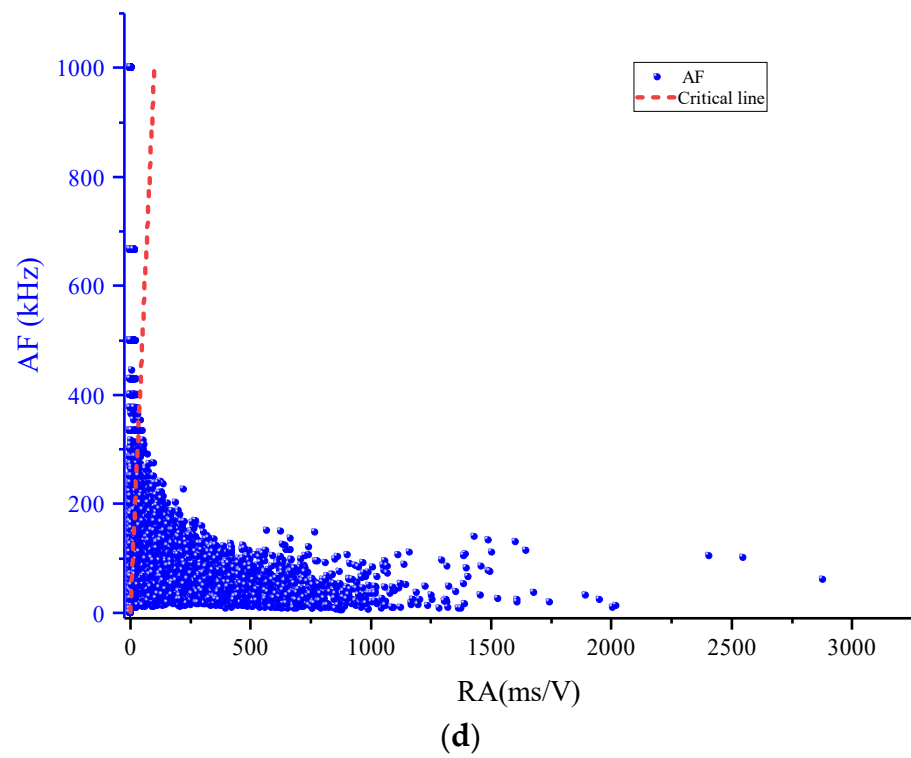


**Figure 17.** Relation between the RA value and the average frequency in direct shear test of binary medium. (a) 8° (b) 30° (c) 45° (d) 55°.

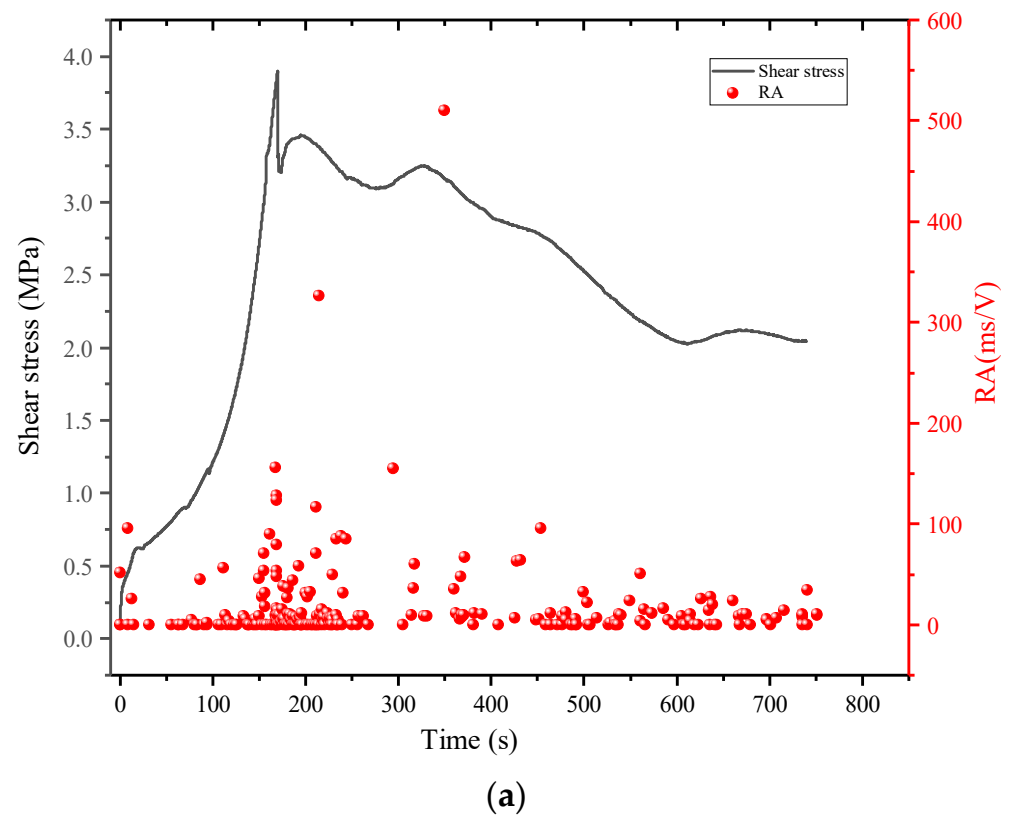


**Figure 18.** Cont.

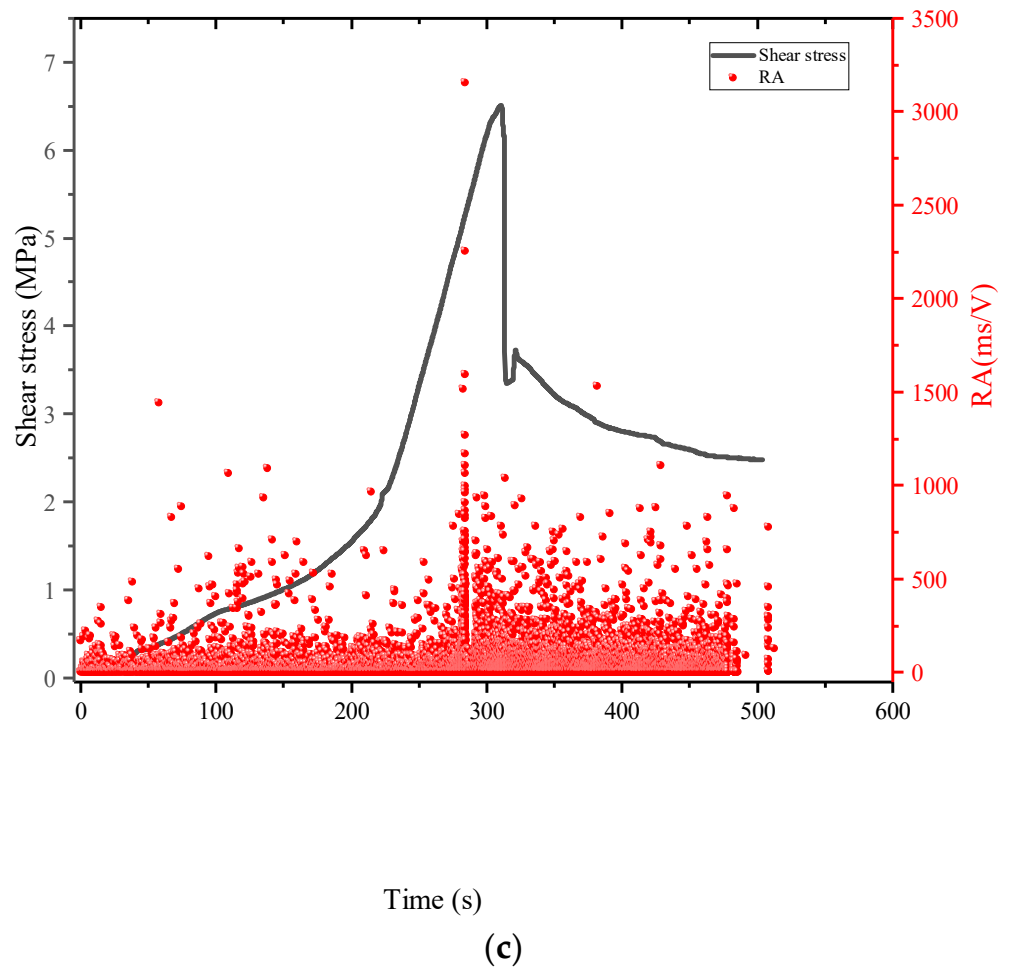
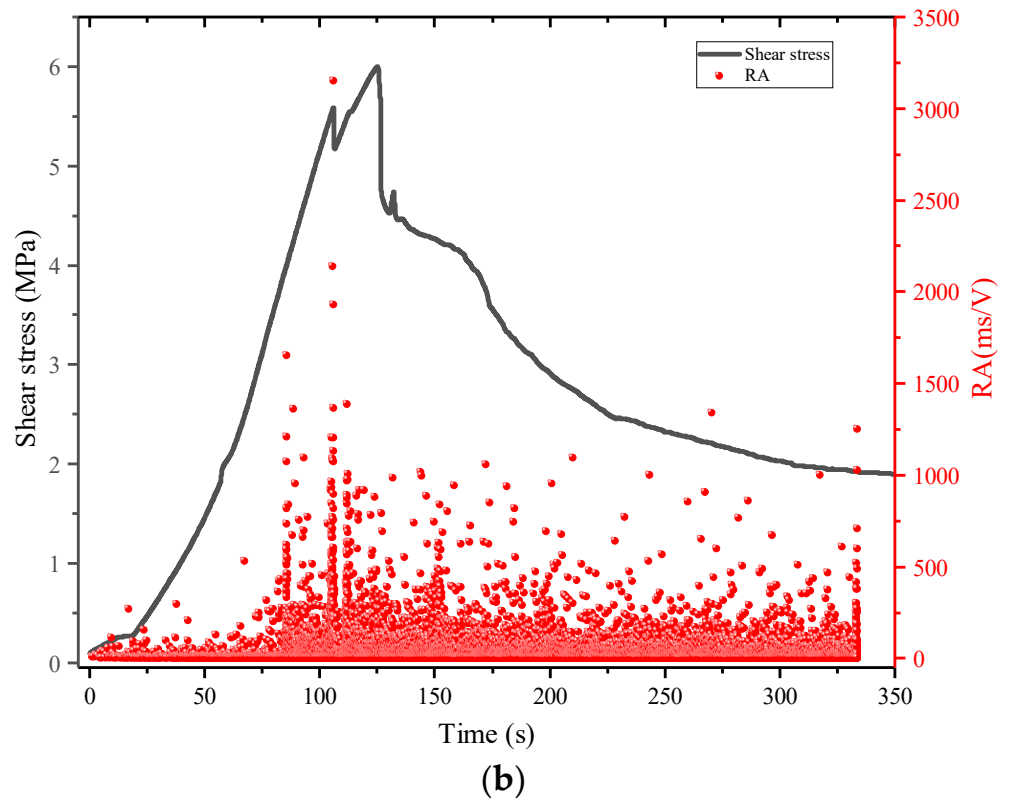
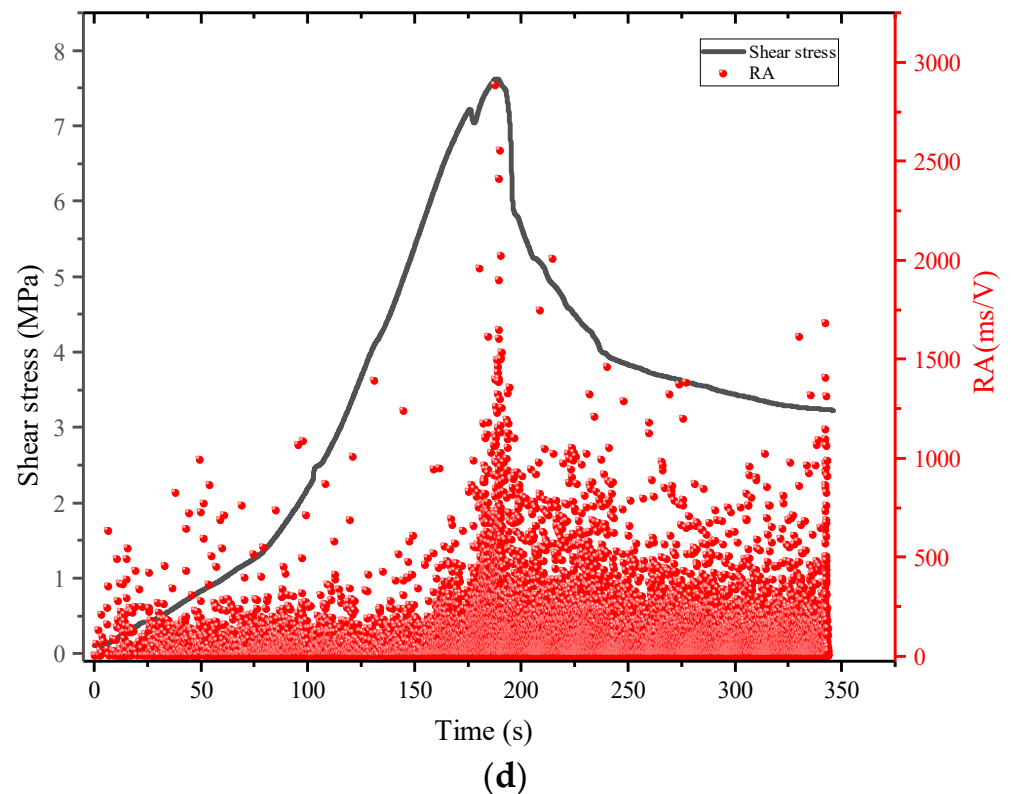
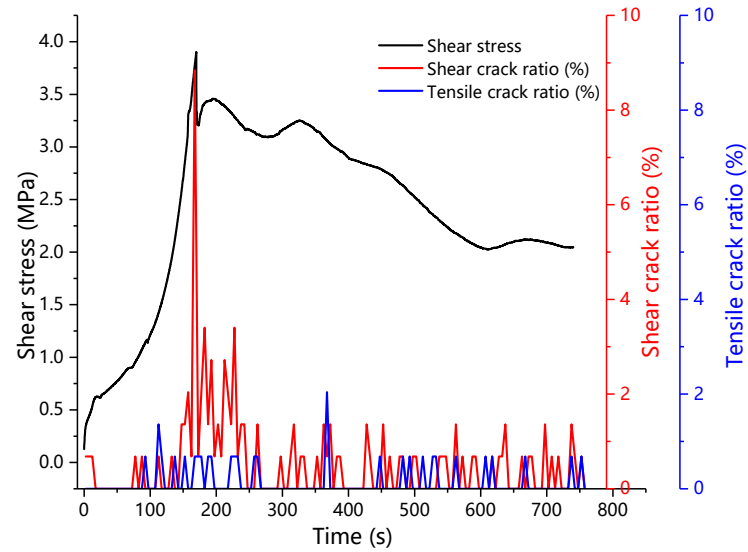


Figure 18. Cont.

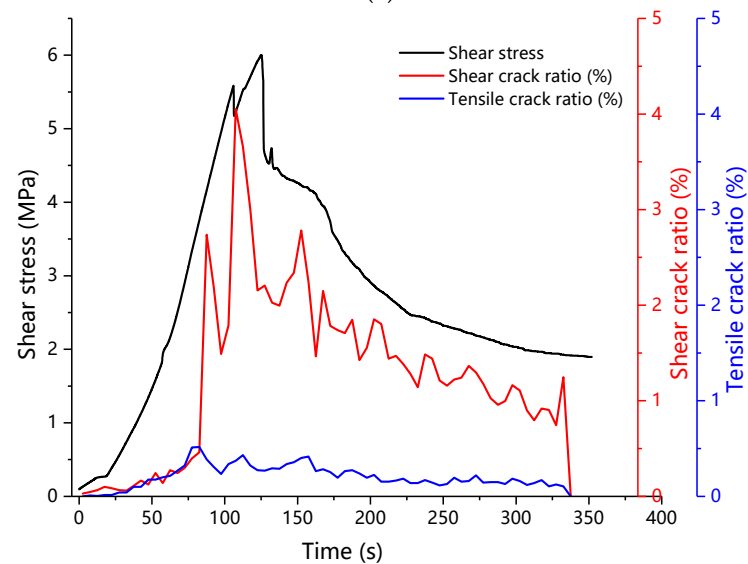


**Figure 18.** Relation between the RA value and the time in direct shear test of binary medium. (a)  $8^\circ$  (b)  $30^\circ$  (c)  $45^\circ$  (d)  $55^\circ$ .

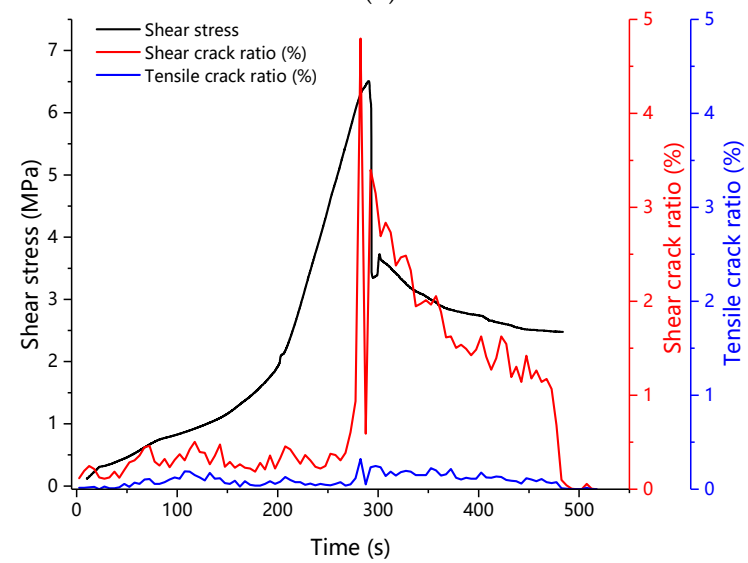
In order to analyze the proportion of shear cracks and tensile cracks in the whole shearing process, Figure 19 shows the proportion of shearing and tensile cracks in all cracks during the shearing process. The red curve in the Figure is the proportion of shear cracks, and the blue curve is the proportion of tensile cracks. It can be seen from the Figure that in most cases, shear cracks are more than tensile cracks, indicating that the tangential stress is the dominant factor leading to the failure of the binary medium in the test, especially in the failure stage and the residual stage. In the shear compaction stage and the elastic stage, the ratio of shear cracks and tensile cracks basically remained stable, but after entering the plastic failure stage, the shear cracks increased suddenly and fell back in the residual stage, but still maintained a high ratio, while the changes in these stages of tensile crack are not obvious. This shows that shear cracks develop violently in the plastic failure stage and residual stage from the aspect of crack ratio, and the main factor leading to structural instability is the development of shear cracks. Corresponding the change of shear crack ratio with the change of shear stress, the sudden increase of shear crack ratio is earlier than the peak of stress, so the sudden increase of shear crack ratio can play a good role in predicting the failure of specimen or structure.



(a)



(b)



(c)

Figure 19. Cont.

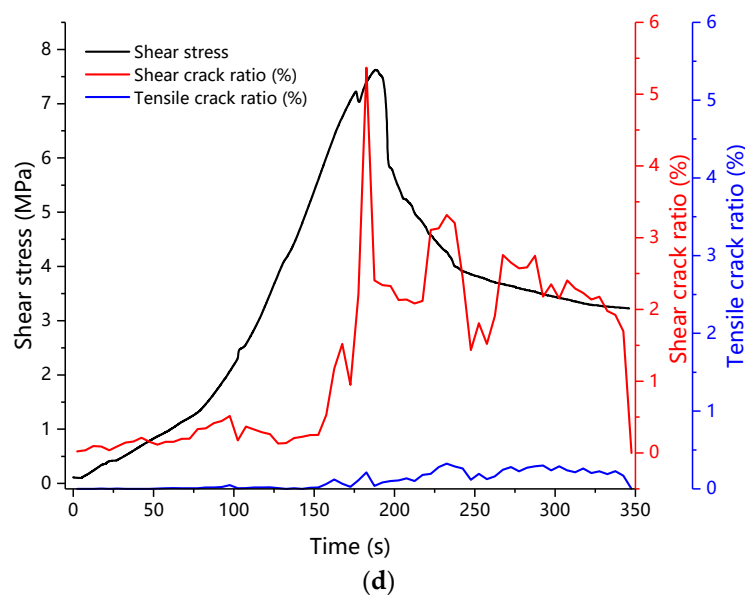


**Figure 19.** Relation between the crack ratio and the time in direct shear test of binary medium. (a)  $8^\circ$  (b)  $30^\circ$  (c)  $45^\circ$  (d)  $55^\circ$ .

### 3.2.4. Peak Frequency Analysis

An acoustic emission signal is a kind of non-stationary signal, and fast Fourier transform (FFT) is a classical spectrum analysis method to analyze a non-stationary signal. The spectral characteristics of the AE signal generated by the rock can characterize the stress state, structure, and mechanical properties of the rock. Many problems that are difficult to visualize in the time domain can be easily identified through acoustic emission spectrum analysis. The peak frequency [33] (in kHz) is defined as the point in the Power Spectrum at which the peak magnitude occurs. A real time FFT is performed on the waveform associated with the AE hit. The peak frequency is the frequency of maximum amplitude [29]. In this paper, the peak frequency information of each sample at different times during the whole loading process is collected, and the variation and distribution of the peak frequency during the shearing process are analyzed. In this paper, the experimental results of the binary medium with the sawtooth angle of  $30^\circ$  and  $45^\circ$  under the normal stress of 3 MPa are selected as the representative for specific analysis. Figure 20 shows the peak frequency changes of the sheared acoustic emission signals of the two samples during the direct shearing process. According to the distribution range and concentrated area of the peak frequency value, the peak frequency distribution map of the whole shearing process is obtained, as shown in Figure 21.

Combining Figures 20 and 21, it can be seen that the peak frequency of the AE signal of the binary medium in the direct shear test is related to the shear stress level. In the shear compaction stage and the elastic stage, the peak frequencies of the AE signal are mainly concentrated in the range of 20–40 kHz and 200–320 kHz. During the plastic failure stage and the residual stage, the peak frequency of the AE signal changed abruptly, with a very large peak frequency, accounting for about 0.01%, and a large number of mid-peak frequencies in the 120–200 kHz frequency band. This indicates that the peak frequency band broadens with the increase of shear stress during the shearing process. M. Cai et al. [19] pointed out that the peak frequency of the AE signal corresponds to small-scale cracks, and the low frequency corresponds to large-scale cracks. Combined with Figure 21, the peak frequency range of the two specimens in the direct shear test is 0–600 kHz, but the peak frequency of 0–340 kHz accounts for more than 99.99%. Therefore, the signal with a peak frequency of around 300 kHz is a high-frequency signal, and the signal with a peak frequency of about 100 kHz is a low-frequency signal. The high-frequency signal and the

low-frequency signal correspond to the micro-crack and through-crack generated in the specimen, respectively.

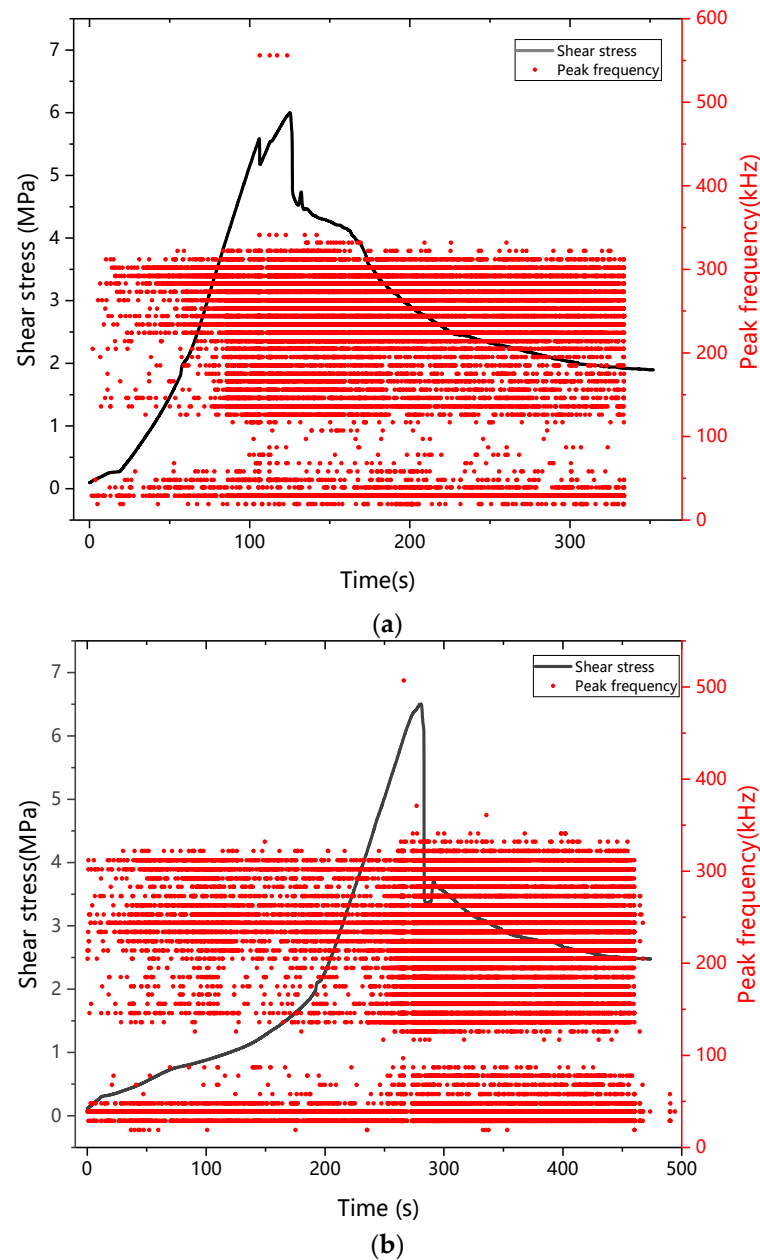


**Figure 20.** Relationship between AE signal peak frequency and time. (a) 30°, (b) 45°.

In order to further analyze the evolution law of the internal fracture of the structural plane at each stage of shearing, the percentage of each frequency interval in each time period was calculated. Figure 22 shows the relation between the percentage of each frequency interval and time. It can be seen from the Figure that the percentage of the signal with a peak frequency of 20–40 kHz is almost unchanged as time increases, indicating that the peak frequency signal of 20–40 kHz is a noise signal due to the equipment or experimental conditions. The peak frequency of the AE signal in the binary medium direct shear test is the high-frequency signal at 220–340 kHz, and the low-frequency signal at 120–220 kHz. In the shear compaction stage, the high-frequency signals tend to increase, and the number of low-frequency signals is much lower than that of the high-frequency signals, and there is almost no change, indicating that a large number of micro-cracks represented by the high-frequency signals are formed. In the elastic stage, the percentage

of high-frequency signals decreased, and the number of low-frequency signals changed little, indicating that under the combined action of normal stress and shear stress, the micro-cracks temporarily closed and suspended development, and no large through cracks were formed. In the plastic failure stage, both high-frequency and low-frequency signals showed a sudden increase, indicating that the micro-cracks rapidly developed and penetrated to form large-scale cracks. And the peak value of the low-frequency signal and the peak value of the shear stress of the specimen occurred synchronously, but the peak value of the high-frequency signal occurred earlier than the two, indicating that the sudden increase of the high-frequency signal is helpful in the prediction of structural instability. In the residual stage, the number of high-frequency and low-frequency signals decreased, but was still much larger than that in the shear compaction stage and the elastic stage, indicating that the slip friction failure caused a large number of micro-cracks and large cracks in the specimen.

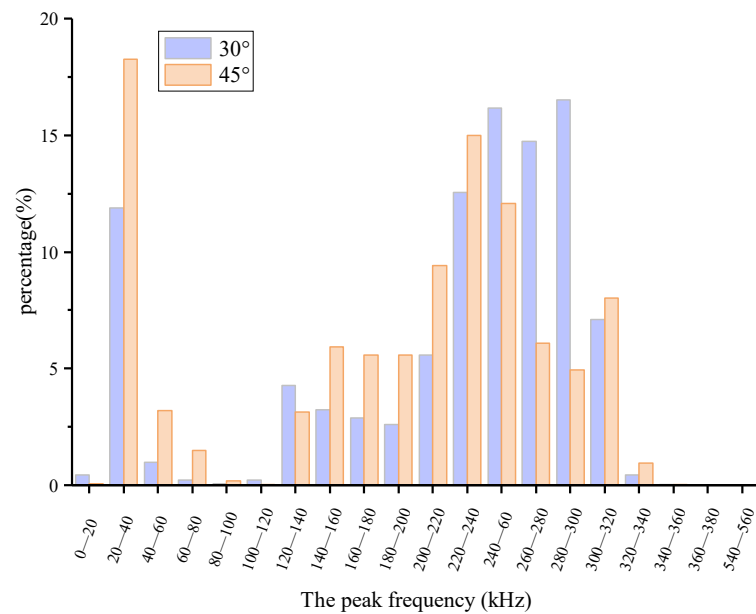


Figure 21. AE signal peak frequency distribution.

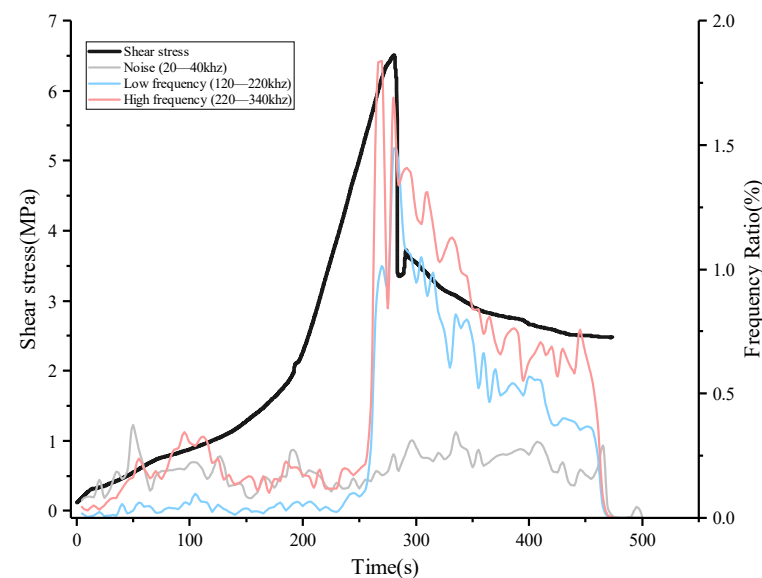


Figure 22. Relationship between peak frequency distribution of AE signal and time.

#### 4. Conclusions

The direct shear test and acoustic emission monitoring of the mortar-rock binary medium with different sawtooth angles were carried out, and the following conclusions were obtained:

1. The direct shear process of the mortar-rock binary medium is divided into five stages. There is a linear relationship between the shear strength of the binary medium and the normal stress, and the relationship between the sawtooth angle and the shear strength of the binary medium, cohesive force, internal friction angle, and residual in-ternal friction angle is established.
2. The AE count and cumulative count of the binary medium direct shear test are both affected by the interface roughness. The greater the sawtooth angle, the greater the AE count and cumulative count.
3. In the plastic failure stage, the AE b value will decrease suddenly, and the proportion of shear cracks in the specimen will increase suddenly. The sudden drop of the AE b value and the sudden increase of the shear crack signal ratio can be used as reference indicators for predicting the macroscopic damage of mortar-rock binary medium.
4. The shear and tensile cracks are distinguished and their proportion is statistically analyzed. With the increase of shear stress, the number of shear cracks increases suddenly, but the change of tensile cracks is little. The development of shear cracks plays a decisive role in the failure of specimens in the shear failure stage. The variation of AE shear crack number can play a role in the early warning and prediction of structural failure. In the practice of monitoring practical engineering, this parameter can be used as one of the parameters to predict structural failure.
5. The peak frequency of shear acoustic emission in the mortar-rock binary medium is distributed in high and low-frequency bands. The effective peak frequency of acoustic emission signal in the direct shear process of binary medium structure is mainly concentrated in 120–340 kHz, and the sudden increase of high-frequency signal (220–320 kHz) has an efficient prediction effect on structural surface damage.

**Author Contributions:** Conceptualization, H.L., W.T.; methodology, W.T.; software, W.T.; validation, Y.C.; formal analysis, W.T.; investigation, J.F.; resources, H.L.; data curation, H.L.; writing—original draft preparation, W.T.; writing—review and editing, Y.C.; visualization, J.F.; supervision, H.H.; project administration, H.H.; funding acquisition, H.H. All authors have read and agreed to the published version of the manuscript.

**Funding:** This paper gets its funding from Hunan provincial key research and development Program (2022SK2082); Science and Technology Project of Hunan Natural Resources Department (2021-52); Science and Technology Progress and Innovation Plan of Hunan Provincial Department of Transportation (201003); Science and Technology Progress and Innovation Plan of Hunan Provincial Department of Transportation (202120); Hunan Civil Air Defense Research Project (HNRFKJ-2021-07). The authors wish to acknowledge these supports.

**Institutional Review Board Statement:** Not applicable.

**Informed Consent Statement:** Not applicable.

**Data Availability Statement:** The data used to support the findings of this study are available from the corresponding author upon request.

**Acknowledgments:** This paper gets its funding from Hunan provincial key research and development Program (2022SK2082); Science and Technology Project of Hunan Natural Resources Department (2021-52); Science and Technology Progress and Innovation Plan of Hunan Provincial Department of Transportation (201003); Science and Technology Progress and Innovation Plan of Hunan Provincial Department of Transportation (202120); Hunan Civil Air Defense Research Project (HNRFKJ-2021-07). The authors wish to acknowledge these supports.

**Conflicts of Interest:** The authors declare no conflict of interest.

## References

1. Han, L.; Lin, H.; Chen, Y.; Lei, D. Effects of strength property difference on shear strength of joint of binary media. *Environ. Earth Sci.* **2021**, *80*, 712. [[CrossRef](#)]
2. Shen, Y.; Wang, Y.; Yang, Y.; Sun, Q.; Luo, T.; Zhang, H. Influence of surface roughness and hydrophilicity on bonding strength of concrete-rock interface. *Constr. Build. Materials.* **2019**, *213*, 156–166. [[CrossRef](#)]
3. Suits, L.D.; Sheahan, T.C.; Seidel, J.P.; Haberfield, C.M. Laboratory Testing of Concrete-rock Joints in Constant Normal Stiffness Direct Shear. *Geotech. Test. J.* **2002**, *25*, 391–404.
4. Zhao, Y.; Chang, L.; Wang, Y.; Lin, H.; Liao, J.; Liu, Q. Dynamic response of cylindrical thick-walled granite specimen with clay infilling subjected to dynamic loading. *Arch. Appl. Mech.* **2022**, *92*, 643–648. [[CrossRef](#)]
5. Fan, X.; Yu, H.; Deng, Z.; He, Z.; Zhao, Y. Cracking and deformation of cuboidal sandstone with a single nonpenetrating flaw under uniaxial compression. *Theor. Appl. Fract. Mech.* **2022**, *119*, 103284. [[CrossRef](#)]
6. Fan, X.; Yang, Z.; Li, K. Effects of the lining structure on mechanical and fracturing behaviors of four-arc shaped tunnels in a jointed rock mass under uniaxial compression. *Theor. Appl. Fract. Mech.* **2021**, *112*, 102887. [[CrossRef](#)]
7. LYBIMOVE, C.; Pinns, E. Crystallization Structure in Concrete Contact Zone between aggregate and cement in concrete. *Colloid J.* **1962**, *24*, 491–498.
8. Qiu, H.; Wang, F.; Zhu, Z.; Wang, M.; Yu, D.; Luo, C.; Wan, D. Study on dynamic fracture behaviour and fracture toughness in rock-mortar interface under impact load. *Compos. Struct.* **2021**, *271*, 114174. [[CrossRef](#)]
9. Chen, L.; Yue, C.; Zhou, Y.; Zhang, J.; Jiang, X.; Fang, Q. Experimental and mesoscopic study of dynamic tensile properties of concrete using direct-tension technique. *Int. J. Impact Eng.* **2021**, *155*, 103895. [[CrossRef](#)]
10. Feng, X.T.; Li, S.J.; Chen, S.L. Effect of water chemical corrosion on strength and cracking characteristics of rocks—A review. In *Advances in Fracture and Failure Prevention, Pts 1 and 2*; Kishimoto, K., Kikuchi, M., Shoji, T., Saka, M., Eds.; Trans Tech Publications Ltd.: Bäch SZ, Switzerland, 2004; pp. 1355–1360.
11. Qiu, H.; Zhu, Z.; Wang, F.; Wang, M.; Mao, H. Dynamic behavior of a running crack crossing mortar-rock interface under impacting load. *Eng. Fract. Mech.* **2020**, *240*, 107202. [[CrossRef](#)]
12. Wang, H.W.; Wu, Z.M.; Wang, Y.J.; Yu, R.C. Investigation on crack propagation perpendicular to mortar–rock interface: Experimental and numerical. *Int. J. Fract.* **2020**, *226*, 45–69. [[CrossRef](#)]
13. Satoh, A.; Yamada, K.; Shinohara, Y. Simulation of Adhesion Performance of Mortar—Mortar Interface with Varied Fractographic Features. *Key Eng. Mater.* **2013**, *577*, 357–360. [[CrossRef](#)]
14. Buzzi, O.; Hans, J.; Boulon, M.; Deleruyelle, F.; Besnus, F. Hydromechanical study of rock-mortar interfaces. *Phys. Chem. Earth.* **2007**, *32*, 820–831. [[CrossRef](#)]
15. Wang, Y.; Chen, S.J.; Zhao, H.T.; Chen, Y.Z. Acoustic emission characteristics of interface between aggregate and mortar under shear loading. *Russ. J. Nondestruct. Test.* **2015**, *51*, 497–508. [[CrossRef](#)]
16. Lin, H.; Zhang, X.; Cao, R.; Wen, Z. Improved nonlinear Burgers shear creep model based on the time-dependent shear strength for rock. *Environ. Earth Sci.* **2020**, *79*, 149. [[CrossRef](#)]
17. Tang, Z.C.; Zhang, Q.Z.; Peng, J.; Jiao, Y.Y. Experimental study on the water-weakening shear behaviors of sandstone joints collected from the middle region of Yunnan province, P.R. China. *Eng. Geol.* **2019**, *258*, 105161. [[CrossRef](#)]
18. Fan, X.; Li, K.; Lai, H.; Zhao, Q.; Sun, Z. Experimental and numerical study of the failure behavior of intermittent rock joints subjected to direct shear load. *Adv. Civ. Eng.* **2018**, *2018*, 19. [[CrossRef](#)]
19. Cheng, Y.; Yang, W.; He, D. Influence of structural plane microscopic parameters on direct shear strength. *Adv. Civ. Eng.* **2018**, *2018*, 7. [[CrossRef](#)]
20. Xie, S.; Lin, H.; Cheng, C.; Chen, Y.; Wang, Y.; Zhao, Y.; Yong, W. Shear strength model of joints based on Gaussian smoothing method and macro-micro roughness. *Comput. Geotech.* **2022**, *143*, 104605. [[CrossRef](#)]
21. Du, S.-G.; Lin, H.; Yong, R.; Liu, G.-J. Characterization of Joint Roughness Heterogeneity and Its Application in Representative Sample Investigations. *Rock Mech. Rock Eng.* **2022**, 1–25. [[CrossRef](#)]
22. Zhao, Y.; Zhang, C.; Wang, Y.; Lin, H. Shear-related roughness classification and strength model of natural rock joint based on fuzzy comprehensive evaluation. *Int. J. Rock Mech. Min. Sci.* **2021**, *137*, 104550. [[CrossRef](#)]
23. Wang, C.; Wang, L.; Karakus, M. A new spectral analysis method for determining the joint roughness coefficient of rock joints. *Int. J. Rock Mech. Min. Sci.* **2019**, *113*, 72–82. [[CrossRef](#)]
24. Lin, Q.; Cao, P.; Cao, R.; Lin, H.; Meng, J. Mechanical behavior around double circular openings in a jointed rock mass under uniaxial compression. *Arch. Civ. Mech. Eng.* **2020**, *20*, 19. [[CrossRef](#)]
25. Naderloo, M.; Moosavi, M.; Ahmadi, M. Using acoustic emission technique to monitor damage progress around joints in brittle materials. *Theor. Appl. Fract. Mech.* **2019**, *104*, 102368. [[CrossRef](#)]
26. 0276.25-2015 DT. Part 25: Test for determining the shear strength of rock. In *Regulation for Testing the Physical and Mechanical Properties of Rock*; Ministry of Land and Resources: Beijing, China, 2015.
27. Ge, Z.; Sun, Q. Acoustic emission characteristics of gabbro after microwave heating. *Int. J. Rock Mech. Min. Sci.* **2021**, *138*, 104616. [[CrossRef](#)]
28. JC MS-III B5706. Monitoring Method for Active Cracks in Concrete by Acoustic Emission. Federation of Construction Materials Industries Japan: Tokyo, Japan, 2003.

29. Physical Acoustics Corporation. *SAMOS AE System User's Manual*; Physical Acoustics Corporation: Princeton Junction, NJ, USA, 2005.
30. Ohno, K.; Ohtsu, M. Crack classification in concrete based on acoustic emission. *Constr. Build. Mater.* **2010**, *24*, 2339–2346. [[CrossRef](#)]
31. Aggelis, D.G. Classification of cracking mode in concrete by acoustic emission parameters. *Mech. Res. Commun.* **2011**, *38*, 3–157. [[CrossRef](#)]
32. Shahidan, S.; Pulin, R.; Bunnori, N.M.; Holford, K.M. Damage classification in reinforced concrete beam by acoustic emission signal analysis. *Constr. Build. Mater.* **2013**, *45*, 78–86. [[CrossRef](#)]
33. Degala, S.; Rizzo, P.; Ramanathan, K.; Harries, K.A. Acoustic emission monitoring of CFRP reinforced concrete slabs. *Constr. Build. Mater.* **2009**, *23*, 2016–2026. [[CrossRef](#)]